Transportation Research Part C 148 (2023) 104041

Contents lists available at ScienceDirect

Transportation Research Part C

journal homepage: www.elsevier.com/locate/trc

A pure number to assess "congestion" in pedestrian crowds

Francesco Zanlungo [a,b,*], Claudio Feliciani [c], Zeynep Yücel [b], Xiaolu Jia [c], Katsuhiro Nishinari [c,d], Takayuki Kanda [e]

[a] International Professional University of Technology in Osaka, 3-1-1 Umeda Kita-ku, Osaka 530-0001, Japan
[b] Graduate School of Natural Science and Technology, Okayama University, 3-1-1 Tsushima-naka Kita-ku, Okayama 700-8530, Japan
[c] Research Center for Advanced Science and Technology, The University of Tokyo, 4-6-1 Komaba, Meguro-ku, Tokyo 153-8904, Japan
[d] Department of Aeronautics and Astronautics, Graduate School of Engineering, The University of Tokyo, 7-3-1 Hongo, Bunkyo-ku, Tokyo 113-8656, Japan
[e] Graduate School of Informatics, Kyoto University, Yoshidahonmachi, Sakyo-ku, Kyoto 606-8317, Japan

ARTICLE INFO

Keywords:
Pedestrian dynamics
Crowd analysis
Simulation
Crowd experiment

ABSTRACT

The development of technologies for reliable tracking of pedestrian trajectories in public spaces has recently enabled collecting large data sets and real-time information about the usage of urban space and indoor facilities by human crowds. Such an information, nevertheless, may be properly used only with the aid of theoretical and computational tools to assess the state of the crowd. As shown in this work, traditional assessment metrics such as density and flow may provide only a partial information, since it is also important to understand how "regular" these flows are, as spatially uniform flows are arguably less problematic than strongly fluctuating ones.

Recently, the Congestion Level (CL), based on the computation of spatial variation of the rotor of the crowd velocity field, has been proposed as an assessment metric to evaluate the state of the crowd. Nevertheless, the CL definition was lacking sound theoretical foundations and, more importantly, was of very difficult interpretation (it was difficult to understand "what" CL was measuring). As we believe that such theoretical shortcomings were limiting also its relevance to applied studies, in this work we clarify some aspects concerning the CL definition, and we show that such an assessment metric may be improved by defining a dimensionless Congestion Number (CN).

As a first application of the newly defined CN indicator we first focus on the cross-flow scenario and, by using discrete and continuous toy models, idealised "limit scenarios", more realistic simulations and finally data from experiments with human participants, we show that $CN \ll 1$ corresponds to a crowd with a regular and safe motion (even in high density and high flow settings), while $CN \approx 1$ indicates the emergence of a congested and possibly dangerous condition. We finally use the CN indicator to analyse and discuss different settings such as bottlenecks, uni-, bi- and multi-directional flows, and real-world data concerning the movement of pedestrians in the world's busiest railway station.

1. Introduction

During the last few centuries, world population has experienced an exponential increase and the steady transition towards urban centres has contributed in further concentrating human population in few densely inhabited areas of the globe. As a consequence,

* Corresponding author at: International Professional University of Technology in Osaka, 3-1-1 Umeda Kita-ku, Osaka 530-0001, Japan.
E-mail address: zanlungo@atr.jp (F. Zanlungo).

https://doi.org/10.1016/j.trc.2023.104041
Received 4 July 2022; Received in revised form 21 November 2022; Accepted 23 January 2023
Available online 4 February 2023

planning and management of human flows within and between urban centres became an increasingly important aspect to ensure both safety and comfort of cities' inhabitants.

While the study of crowds and their dynamics is not a new topic (for example, the Colosseum of the Roman Empire was supposedly built to also take into account crowd motion during evacuations (Elliott and Smith, 1993; Vendelø, 2019)), the approach taken in regard to pedestrian traffic has been greatly influenced by available knowledge and technologies. In the 19th century, pedestrian facilities, such as train stations or stadia were mostly built based on previous experience on pedestrian traffic and putting focus on structural stability, functionality or appearance. During the 20th century, accidents occurring due to poor crowd management or related to the failure in considering occupants as an integral part during the design process led to the necessity to create clear standards in relation to pedestrian traffic (Elliott and Smith, 1993; Rogsch et al., 2010; Illiyas et al., 2013).

In the second half of the 20th century, with the appearance of numerical computing, building structural calculations were greatly simplified by the availability of architectural software. Nowadays, it is also possible to simulate smoke spread in case of fire and predict people movements using commercial software (Munirajulu, 2018; Lovreglio et al., 2019), thus allowing to verify whether a structure will be able to ensure safety standards in case of evacuation. At the same time, the appearance of video cameras allowed to collect recordings of pedestrian flows to be later analysed in detail (Weidmann, 1993; Cheung and Lam, 1998; Lam and Cheung, 2000). This increased amount of data allowed to define better and more accurate standards, and quantities such as the Level of Service (LOS) (Fruin, 1971) started to emerge as potential indicators in regard to the quality of public spaces from the point of view of its pedestrian users.

As a consequence of the knowledge gained from past accidents and the norms implemented to avoid their re-occurrence, crowd accidents are now rare in facilities specifically designed to accommodate large crowds, yet they still occur (e.g. the Love Parade accident or the several tragedies which occurred during Hajj). This shows that constant monitoring during mass events is necessary to fill planning gaps or to deal with unexpected/unpredicted conditions. However, simply employing a large number of cameras makes it difficult to have an overall view on the situation and, therefore, developing indicators helping security personnel to identify risky locations should be an important goal of crowd research. In 2015, 27 pilgrims were killed in a dense crowd during a religious event in India, despite the fact that 15'000 policemen and 171 cameras were reportedly used to monitor the event (Ravishankar et al., 2015). This also shows the challenges posed by events held over a short time in temporary facilities, where simulation conditions are difficult to be set up and the possibility of structural modifications is limited or absent (Illiyas et al., 2013; Wikipedia, 2020).

Over the last few decades, technology has made big progresses and it is now possible to detect and track pedestrian positions in real-time (Masoud and Papanikolopoulos, 2001; Szarvas et al., 2006; Zanlungo et al., 2015; Corbetta et al., 2018) (although for dense crowds this is still a challenging task) and also to gain additional information such as height (Brščić et al., 2013), body temperature (Lin et al., 2019), gender (Cai et al., 2018), the presence of a luggage (Atienza-Vanacloig et al., 2008), groups and their social relation (Yücel et al., 2013, 2019). Such sensors and algorithms provide information on crowd features which are known to affect the microscopic pedestrian behaviour, although their influence on macroscopic crowd dynamics is still not completely understood (Brščić et al., 2014; Zanlungo et al., 2017, 2019b)

Under this perspective, the collection of data to define new norms to be used for pedestrian traffic is slowly playing an increasingly less important role within crowd management studies (Haghani, 2020a,b). The decreasing number of accidents in certified and well-managed facilities show that existing norms are possibly already satisfactory. On the other hand, the availability of real-time data on crowd motion has posed new challenges in regard to the assessment of crowd dynamics in real-time, with definitions like the LOS becoming inadequate for a real-time flexible use (remember that LOS is defined for specific structures and it may not always be easy to find a match in complex facilities).

The increased amount of data is also changing the approach on crowd management. Although, until recently, a continuous check of multiple surveillance cameras by security staff was the only means to evaluate crowd motion, as already mentioned, now tracking technologies also allow to extract pedestrian position, with additional technologies (GPS, Bluetooth scanners, inertial sensors, etc.) providing complementary information (Van der Spek et al., 2009; Schauer et al., 2014; Boltes, 2015; Feliciani and Nishinari, 2018a). How to use such information to quantitatively measure properties related to crowd dynamics is now of utmost importance, since a successful evaluation of crowd conditions would allow a real-time assessment, thus potentially preventing accidents also in case of unpredicted behaviours.

Despite the importance attributed to the numerical assessment of crowd conditions, little research has been addressed on this topic. Speed and density are still the most broadly employed quantities to estimate the state of the crowd and although they are sufficient and adequate in most of the cases, they also have limitations given by the fact that they are simple adaptations of physical principles to crowd motion, thus not taking into account the human peculiarities of pedestrian dynamics. Several studies have tried to provide a quantitative estimator for the state of the crowd, but in most of the cases the measures introduced were intended to describe a particular aspect related to a specific experimental configuration (like the order parameter (Nowak and Schadschneider, 2012) or the band index (Yamori, 1998)) and only few were aiming towards a universal application to real pedestrian environments.

Among the quantities introduced to describe crowd motion, two types can be distinguished: physical approach and data-driven approach. Physical approaches are based on physical laws, which are adapted to take into account peculiarities of human motion (such as the "crowd turbulence" (Helbing et al., 2007) or the "velocity entropy" (Huang et al., 2015)), while data-driven approaches employ machine learning algorithms to assess videos or data set based on training data. In this work, we focus on the former approach as it allows to gain knowledge on pedestrian motion, it is computationally more efficient and more suited for a general quantification of crowd motion. We nonetheless recognise the importance and relevance of machine learning approaches to detect for example violence (Nievas et al., 2011; Hassner et al., 2012) or specific features of human behaviour (Kratz and Nishino, 2009; Kok et al., 2016).

In an attempt to define a universal indicator for the "smoothness" of crowd motion[1] solely based on the velocity vector field (which can be easily obtained for crowds of different densities with little computational cost), the so-called congestion level (CL) was introduced by Feliciani and Nishinari (2018b). However, despite having proved being a useful and valid method to evaluate different types of pedestrian motions Feliciani et al. (2018), Fujita et al. (2019), Feliciani and Nishinari (2020), Feliciani et al. (2020b), Ye et al. (2020, 2021) and Hosseini et al. (2021), the original formulation lacked in theoretical integrity, mostly with respect to three important issues:

- The CL, which is defined as the ratio of the difference between the maximum and minimum value of the velocity rotor magnitude in a given "region of interest" to the average speed in the same region (see Eq. (1) for a formal definition), takes the unit of m^{-1}. Universal quantities used in physics are however typically dimensionless (consider for example the Reynolds or the Mach number), thus hindering the physical validity of the CL in its original definition. Furthermore, as we discuss below, the CL has an explicit dependence on the choice of a computational parameter, namely the size of the grid used for the computation of the velocity field.
- In the original work (Feliciani and Nishinari, 2018b), it is argued that a crowd moving in normal conditions (i.e., not in a state of fear or emergency, such as when trying to escape a fire) would never exceed a CL of 15 m^{-1}. Although this value was obtained by extrapolation from experimental data, it remains a hypothesis and it would be difficult to demonstrate the existence of a limit experimentally due to safety and ethical limitations. As such, a general, universal and preferentially theoretical argument is required to demonstrate such a limit and quantify it numerically.
- Since the CL was originally conceived to be used on discrete experimental data, a continuous definition has not been provided. Although a continuous definition is not strictly necessary, its existence would allow to better investigate the properties and the limitations of the CL without the need of experimental data.

In this work, we attempt to solve the issues discussed above and present a pure (dimensionless) number, which we define as "congestion number" (CN), based on accepted physical and mathematical principles, while taking into account the properties of humans and their collective dynamics inside a crowd. We normalise CN in such a way that, in normal conditions, it takes positive values smaller than 1; the value 1 being approached or exceeded only in emergencies or extraordinary events.

To better study the properties of the newly defined CN, we first focus on a cross-flow scenario, which we believe, for the reasons explained in Appendix A, to be the most appropriate to study the features of the proposed indicator. To this purpose, we first use numerical simulations to investigate, on one hand, conditions in which the pedestrian flows are basically non-interacting and thus for which we expect very low CN values (as the flow is by definition "non-disrupted") and, on the other hand, conditions in which the flows are critically disrupted and thus we expect $CN \approx 1$. Simulations are necessary to attain this goal, since in order to have high density but not interacting flows we need to introduce artificial pedestrian motion rules; furthermore, simulations are also necessary to create extremely disrupted conditions without affecting the safety of human subjects. We also analyse a controlled cross-flow experiment with human participants under challenging but safe conditions, for which we expect intermediate CN values.

After the main properties of the CN indicator have been analysed on the cross-flow scenarios, we briefly show how it can be applied to various settings, such as bottlenecks, uni-, bi- and multi-directional flows, and real-world data concerning the movement of pedestrians in a large scale railway station. A final example, focusing on a bi-directional flow over a loop, is used to highlight the ability of the CN indicator to differentiate "regular" (self-organised) crowd movements from less organised ones even when density and velocity patterns are very similar.

1.1. Outline of this article

In Section 2 we review the original definition of CL, while in Section 3 we define our new indicator, CN. Section 4 focuses on the numerical study of the cross-flow scenario, while in Section 5 we analyse the controlled cross-flow experiment. In Section 6 we use the CN crowd indicator to analyse a variety of experimental and real-world settings.

Finally, the Appendices focus on subjects such as the reason to analyse mainly the cross-flow scenario A, the reason to use the term "congestion" in the name of the indicator B, the choice of computational parameters C, and finally a discussion of discrete and continuous toy models of high CN settings D.

2. Definition of congestion level and related issues

2.1. Definition

Let us first recall the definition of Congestion Level: assuming a field of pedestrian (crowd) velocity $\mathbf{v}$ is given, we may define on a point $\mathbf{x} = (x, y)$ of planar space

$$CL(\mathbf{x}) = \frac{\max_{R(\mathbf{x})}(\nabla \times \mathbf{v})_z(\mathbf{x}) - \min_{R(\mathbf{x})}(\nabla \times \mathbf{v})_z(\mathbf{x})}{\langle v \rangle_{R(\mathbf{x})}}. \tag{1}$$

[1] By smoothness here we roughly mean the ability of pedestrians to follow their preferred path without strong local deviations from it; since such individual paths are unknown, we try to recover this information from an analysis of the velocity vector field at the crowd level.

In this equation, v stands for the magnitude of the velocity field, extrema and averages are computed over a Region Of Interest (ROI) centred around $\mathbf{x}$, and denoted as $R(\mathbf{x})$, while $(\nabla\times\mathbf{v})_z$ denotes the z component of the rotor of the velocity field (i.e., the only non-zero component). We remind the readers that the numerator is defined as "Rotation Range", while "Crowd Danger" is defined as the product of CL and crowd density (Feliciani and Nishinari, 2018b), although we do not consider these important assessment metrics in this work.

Obviously, defining a velocity field for a crowd is not a trivial issue, as it involves problems related to the characteristic scales of crowd dynamics. Indeed, any "fluid dynamics" approach to crowd dynamics involves nontrivial problems, since often the interesting scale of the problem (e.g., corridor width) is very similar to that of the basic component of the crowd (humans), and in general the conditions usually required for using a continuous physics approach (Lautrup, 2011) are not satisfied. Although these problems are extremely relevant to the following discussion, for technical details such as choosing the correct time and space smoothing tools to define the velocity field from tracking trajectories, we refer the reader to the original work (Feliciani and Nishinari, 2018b).

2.2. Issues

In this work, we are interested in two possible problems with this definition, and namely:

1. CL is not a pure number, and for this reason it does not have an easy to interpret scale (its dimension is $[L]^{-1}$, i.e. the inverse of a length),
2. The definition mixes local (differential) quantities such as the rotor with global ones (extrema, averages), which, along with the original problems in definition of a velocity field (or, equivalently, of a density field), makes again its interpretation difficult.

Concerning the physical dimension aspect, it should be noticed that, being the ratio between the variation of the velocity rotor and the average velocity, CL is left unchanged by a re-scaling of the velocity field. As a result, changing the time units does not change the CL value (since both the numerator and denominator are scaled by the same factor, or, in an equivalent way, since CL has no dimensional dependence on time). This also means that a high velocity field and a low velocity field have the same CL value, if they are just obtained through a constant (over space) scaling. This may seem counter-intuitive, but it is actually a nice property of the CL concept, as we discuss in our analysis of simulated data in Section 4. This does not, obviously, imply that crowd velocity is not relevant to crowd risk. It has to be expected that relatively simple measures may not fully take in consideration every aspect of crowd risk, and CL should be always used along other measures that may take velocity in consideration.

On the other hand, CL changes if we change the spatial units, or, in an analogous way, if the spatial properties of the field are scaled. As the original definition introduces a spatial scale, i.e. the grid size R, the dimensionless product $R\cdot CL$ should be expected to be related to a meaningful definition of a crowd assessment metric. Let us see how to formalise this idea.

3. Definition of a congestion number

3.1. Relation to the rotor gradient (differential congestion)

As stated above, Feliciani and Nishinari (2018b) provide a detailed discussion on the scales at which the grid for the velocity field and the ROI should be computed to obtain results that are significant and useful from a crowd management point of view (for a further discussion, see Appendix C). It seems reasonable that the ROI should be large enough to be able to assess the change in the z component of the rotor, but not too large, as this would lead to an underestimate of the rate of change. Namely, assuming L to be the linear scale of the ROI, we may use a linear approximation

$$\max_{R(\mathbf{x})}(\nabla\times\mathbf{v})_z(\mathbf{x}) - \min_{R(\mathbf{x})}(\nabla\times\mathbf{v})_z(\mathbf{x}) \approx L\|\nabla[(\nabla\times\mathbf{v})_z(\mathbf{x})]\|. \tag{2}$$

We may now see that the CL numerator is proportional, according to the proposed approximation and interpretation, to the magnitude of a differential operator applied on the velocity field, namely the gradient of the only non-zero component of the rotor of the velocity field. We may call the latter Differential Congestion (DC), namely

$$DC(\mathbf{x}) = \|\nabla[(\nabla\times\mathbf{v})_z(\mathbf{x})]\|. \tag{3}$$

3.2. Congestion number as a ratio with an extreme differential congestion

We still need to explain the remaining terms. The proposed explanation is that congestion is indeed related to DC, but the remaining terms arise by taking a ratio between the measured DC and a reference value, that we may call Extreme Differential Congestion, or EDC. Such a ratio is obviously a pure number, which we may call Congestion Number (CN)

$$CN(\mathbf{x}) = \frac{DC(\mathbf{x})}{EDC(\mathbf{x})}. \tag{4}$$

In the following, we are going to define EDC (which still depends on $\mathbf{x}$, as it is related to the local magnitude of the velocity) and derive the relation between CL and CN.

3.3. Definition of extreme differential congestion

To introduce a "maximally rotating field", let us first recall the usual "elementary" definition of Stokes' theorem in classical vector analysis[2]

$$\int_S (\nabla \times \mathbf{v}) \cdot \mathbf{dn} = \int_C \mathbf{v} \cdot \mathbf{dl}, \tag{5}$$

where the 1-D path C is the boundary of the 2-D region S. For a circular path of radius R, denoted as C_R, over which the magnitude of the velocity field is fixed to a constant value, v_R, the maximum value for the integrals defined above is given by a field exactly directed along the tangent to the path

$$\mathbf{v}(R, \varphi) = v_R \mathbf{e}_\varphi, \tag{6}$$

where $\mathbf{e}_\varphi$ is the angular versor whose Cartesian components are $(-\sin\varphi, \cos\varphi)$ or $(-y/r, x/r)$. For this field, we have

$$\int_{D_R} (\nabla \times \mathbf{v}) \cdot \mathbf{dn} = \int_{C_R} \mathbf{v} \cdot \mathbf{dl} = 2\pi v_R R, \tag{7}$$

regardless of the value attained inside the disc D_R. Obviously, the reversed field $-v_R \mathbf{e}_\varphi$ assumes the minimum value $-2\pi v_R R$.

We may choose the values assumed inside D_R by requiring the field to go continuously and linearly to 0 towards the centre

$$\mathbf{v}(r, \varphi) = v_R \frac{r}{R} \mathbf{e}_\varphi. \tag{8}$$

For this field, the non-zero component of the rotor is given by the cylindrical coordinate formula

$$(\nabla \times \mathbf{v})_z = \frac{1}{r} \partial_r \left(r v_R \frac{r}{R} \right) = \frac{2 v_R}{R}, \tag{9}$$

or, equivalently, by

$$\partial_x v_y - \partial_y v_x = (\partial_x x - \partial_y (-y)) v_R / R = 2 v_R / R. \tag{10}$$

The original formula for CL includes the average value of v over the ROI, and for this reason it may be useful to compute the average value of v over D_R, which is

$$\langle v \rangle_{D_R} = \frac{\int_{D_R} v}{\pi R^2} = \frac{\int_{D_R} v_R \frac{r}{R}}{\pi R^2} = \frac{\int_0^{2\pi} \mathrm{d}\varphi \int_0^R r v_R \frac{r}{R} \mathrm{d}r}{\pi R^2} = \frac{2\pi \frac{v_R}{R} \int_0^R r^2 \mathrm{d}r}{\pi R^2} = \frac{2 v_R}{R^3} \frac{R^3}{3} = \frac{2}{3} v_R, \tag{11}$$

or

$$v_R = \frac{3}{2} \langle v \rangle_{D_R}. \tag{12}$$

Substituting in Eq. (9) we obtain

$$(\nabla \times \mathbf{v})_z = \frac{2 v_R}{R} = \frac{3 \langle v \rangle_{D_R}}{R}. \tag{13}$$

These considerations on vector analysis are obviously independent of pedestrian dynamics. Let us now assume that the maximum value for the rotor in a pedestrian velocity field is given when a maximally rotating field, as defined above, occurs on a scale comparable to the pedestrian body size, $R \approx 0.2$ m, which is incidentally the value chosen by Feliciani and Nishinari (2018b) for the size of the cell grid.[3]

We now define the EDC as a gradient corresponding to a change from two different but opposite maximally rotating fields located at a distance L, which corresponds to the linear size of the ROI. Namely,

$$EDC = \frac{\frac{3\langle v \rangle_{D_R}}{R} - \left(-\frac{3\langle v \rangle_{D_R}}{R}\right)}{L} = \frac{6 \langle v \rangle_{D_R}}{RL}. \tag{14}$$

We will again consider later the relation between this "approximated macroscopic gradient" and the actual local gradient defined on a continuous field, see in particular Appendix D.

Furthermore, we are going to assume that the average of the magnitude of vector field on the ROI is equivalent to that of the average over the maximally rotating area, which leads to

$$EDC(\mathbf{x}) \approx \frac{6 \langle v \rangle_{R(\mathbf{x})}}{RL}. \tag{15}$$

Again, we discuss this approximation in Appendix D.

[2] This result is a special case of the more general differential geometry theorem due to Cartan, see for example (Frankel, 2011).

[3] Readers may notice that for defining the maximally rotating vector field we used a continuous field defined obviously at a scale much smaller than R; we will come back on this issue in Appendix D.

3.4. Operational definition of CN

Recalling our definition of CN, Eq. (4), and the approximation Eq. (2), we have

$$CN(\mathbf{x}) \approx \frac{(\max_{R(\mathbf{x})}(\nabla \times \mathbf{v})_z(\mathbf{x}) - \min_{R(\mathbf{x})}(\nabla \times \mathbf{v})_z(\mathbf{x}))RL}{6\langle v \rangle_{R(\mathbf{x})} L}, \tag{16}$$

or

$$CN(\mathbf{x}) \approx CL(\mathbf{x})\frac{R}{6}, \tag{17}$$

which may be also considered as the operational definition of CN. Eq. (17) thus implies that the operational definition of CN simply boils down to an R-dependent linear scaling of CL.

According to this derivation, in the experiments reported by Feliciani and Nishinari (2018b), maximum registered values of CN would be around 0.5. It looks clear that values of $CN \ll 1$ should correspond to non-congested crowds, while as CN gets comparable to 1, the crowd should be extremely congested. Nevertheless, it should be noticed, as we discuss in detail in Appendix D, that values of $CN > 1$ are attainable, since it is possible to define fields for which the DC is larger than the proposed EDC. Anyway, as the maximum possible DC depends on the discretisation and numerical scheme, and corresponds to highly artificial settings, we do not try to define CN in such a way that $0 \leq CN \leq 1$ always holds.

For a better clarification of the meaning of these definitions through explicit (discrete and continuous) models, along with a discussion of numerical computation details, the reader is referred to Appendix D. The appendix provides also a justification for the choice of the ROI size used in this work and by Feliciani and Nishinari (2018b) and Feliciani and Nishinari (2020).

4. Simulations

Let us now study some interesting properties of this assessment metric when applied to a crowd system. As a first step, we want to test the CN indicator under some extreme conditions which may be better attained by using simulations. Here we decided to compute CN in each cell, including those that do not present non-zero velocity and/or do not have a defined rotor field; obviously such cells have a non-zero CN only if in their ROI there is a non-zero rotor cell. The ROI was chosen as a Euclidean $D_{7/2R}$, refer to Appendix D for details. All the computations reported in this work have been obtained using the code accessible at Zanlungo (2020).

The studied problem is the intersection of two corridors (width of 3 m), each one with a high density/high flux uni-directional flow in it. We use three approaches for "simulating" this system

- "Centralised marching rule": the velocity and position of the pedestrians are decided in advance in a centralised way, such that even at a density as high as 9 pedestrians per squared metre the pedestrians do not need to slow down (an example for such a marching line-up is given in Rokko High School (2017)). Two uni-directional flow densities are proposed: ≈ 2 and ≈ 4.5 (Fig. 1) ped/m^2, while the walking velocity is fixed to 1 m/s, using respectively 408 and 816 pedestrians.[4] A similar rule, "stripe formation", may also be used by self-organising agents (Zanlungo, 2007), but in realistic settings the resulting patterns would be unstable and emerge as the result of continuous interaction between the pedestrians. On the other hand, when the relative positions and velocities are fixed in advance, there is no actual interaction and by definition no disruption; we thus expect to attain low CN values despite the high density flow. We refer to this simulation setting as "Marching".
- "Non-interacting particles drifted random walk": each pedestrian has a different velocity (from a Gaussian distribution centred on 1 m/s with $\sigma = 0.1$ m/s) and performs a "drifted random walk" towards its goal. Nevertheless, physical dynamics is performed in the zero body size limit (collisions happen only with the walls) and pedestrians do not perform collision avoidance. Two uni-directional flow densities are proposed: 2 and 4 (Fig. 2) ped/m^2, using respectively 408 and 816 pedestrians. Also in this simulation setting there is, by definition, no interaction and we thus expect a low CN. We introduce it to verify whether we can have low CN also in presence of random noise. We refer to this simulation setting as "zero body size".
- "Finite body size": simulated pedestrians have rigid bodies with a fairly realistic size and shape (ellipses with axis $a = 0.45$ m and $b = 0.2$ m) and perform collision avoidance according to the model described by Zanlungo et al. (2019a). Two uni-directional flow densities are proposed: 1 (Fig. 3) and 2 (Fig. 4) ped/m^2, using respectively 128 and 256 pedestrians. The initial density conditions for "finite body size" pedestrians are thus lower than those used for "marching" and "zero body size" ones, but since the "finite body size" case involves an actual congestion problem, density values similar to those of the "marching" and "zero body size" settings are assumed in the crossing area. Velocities are drawn from a Gaussian distribution with mean 1 m/s and $\sigma = 0.1$ m/s.

  In this setting pedestrians perform some level of collision avoidance, nevertheless their behaviour should not be considered as particularly realistic since the model parameters had not been calibrated on actual pedestrian dynamics, and the purpose of the "finite body size" simulation *is not to reproduce realistic human behaviour* (realistic human behaviour is studied in Section 5 by analysing directly human pedestrian data without relying on simulations). On the other hand, this simulation approach is used *to artificially create an extremely "congested" crowd setting*, and study the properties of CN in such a condition.[5]

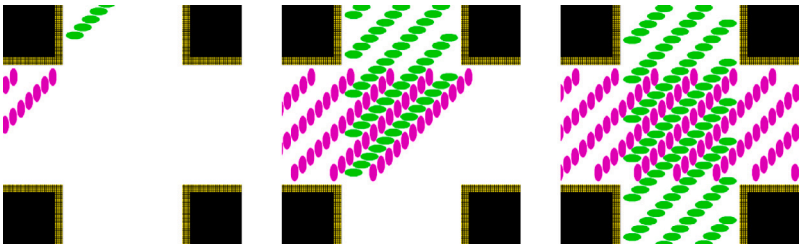

Fig. 1. Snapshots (time increasing from left to right) for "marching" pedestrians, uni-directional flows with 4.5 ped/m^2 initial density.

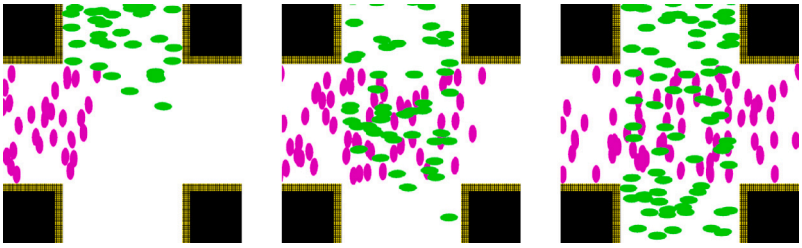

Fig. 2. Snapshots (time increasing from left to right) for "zero body size" pedestrians, uni-directional flows with 4 ped/m^2 initial density.

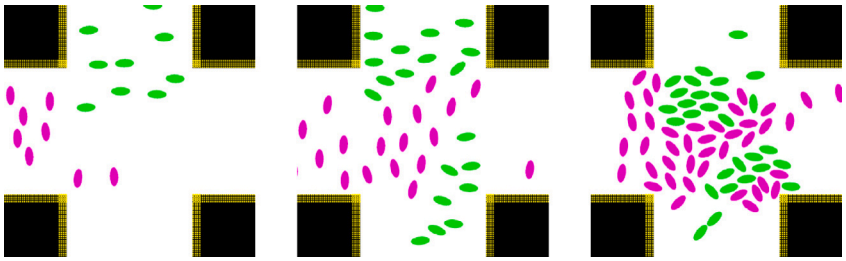

Fig. 3. Snapshots (time increasing from left to right) for "finite body size" pedestrians, uni-directional flows with 1 ped/m^2 initial density.

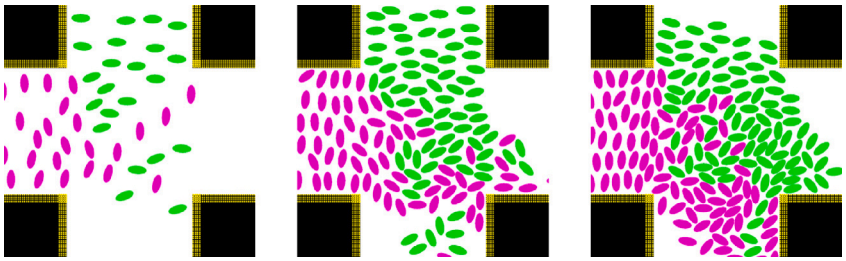

Fig. 4. Snapshots (time increasing from left to right) for "finite body size" pedestrians, uni-directional flows with 2 ped/m^2 initial density.

CN is a local indicator (i.e., defined at a given time and point in space), nevertheless crowd phenomena develop over a finite area and time interval. To better assess the relation between the CN indicator and crowd dynamics, we are going to study the time dependence of the following variables:

1. $\langle\rho\rangle(t)$, the (spatial) average pedestrian density in the crossing area, computed as a function of time. We consider this CN-unrelated variable due to its practical and historical relevance in pedestrian studies.[6]

[4] These specific numbers were chosen based on the geometry of the problem in order to "fill" the diagonal lanes visible in Fig. 1.

[5] We refer readers interested in reproduction of crowd dynamics in a cross-flow scenario through computational models to Zanlungo et al. (2023b).

[6] $\langle\rho\rangle$ is simply defined by counting the number of pedestrians in the crossing zone and dividing by the area. Details of the computational method may be found in the code accessible at Zanlungo (2020). The same observable is also analysed by Zanlungo et al. (2023a), which provides a detailed definition.

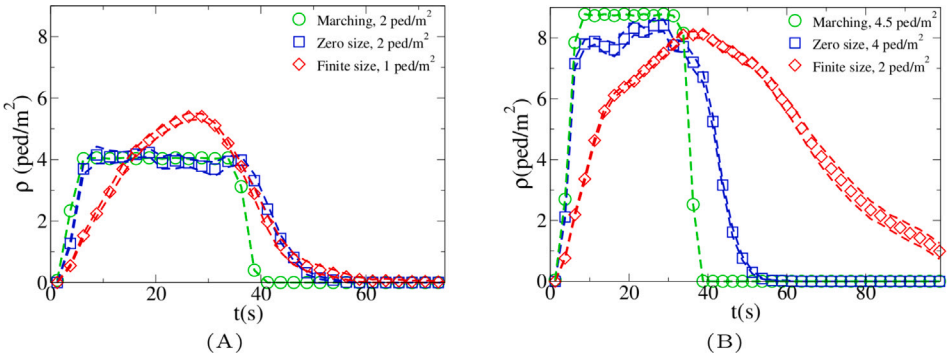

Fig. 5. Average density $\langle\rho\rangle(t)$ in the crossing area as a function of time for all density scenarios ((A): lower density initial conditions; (B): higher density initial conditions). Densities are averaged over 10 different randomly chosen initial conditions (excluding for the deterministic "marching" settings) and on time intervals of 2.5 s. Dashed lines provide standard error intervals.

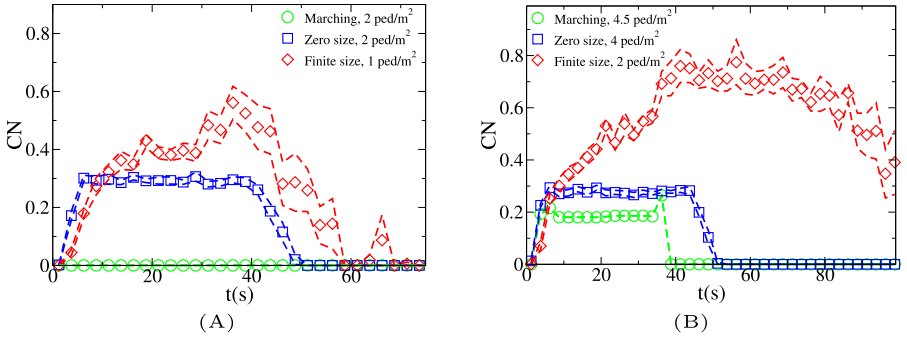

Fig. 6. $CN^M(t)$ (maximum CN over all cells, averaged over 10 different randomly chosen initial conditions) as a function of time for all density scenarios ((A): lower density initial conditions; (B): higher density initial conditions). Dashed lines provide standard error intervals.

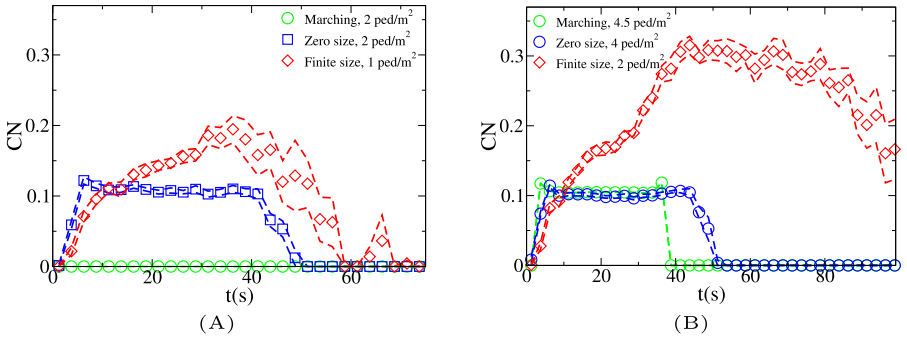

Fig. 7. $\langle CN\rangle(t)$ (computed as an average over non-zero CN cells, and averaged over 10 different randomly chosen initial conditions) as a function of time for all density scenarios ((A): lower density initial conditions; (B): higher density initial conditions). Dashed lines provide standard error intervals.

2. $CN^M(t)$, the maximum value attained by CN (maximum over all cells, computed as a function of time).
3. $\langle CN\rangle(t)$, the average value of CN over cells with non-zero CN value (computed again as a function of time).

$\langle\rho\rangle(t)$ is shown for each setting and model in Fig. 5. Unidirectional flows and conditions have been chosen in such a way to have similar density peak values, and similar crossing time scales in each one of the "lower density" and "higher density" settings for all models. Anyway, since 128 "finite body size" pedestrians need roughly the same time to clear the crossing area as 408 "zero body size" ones, and 256 "finite body size" ones double the time needed by 816 "zero body size" ones, it is clear that the flux (and velocity) is significantly decreased in the "finite body size" case. Despite this, as shown in Fig. 6, $CN^M(t)$ attains a higher value in "finite body size". In this (recognising the crowd congestion regardless of a slower velocity/lower flux) clearly the velocity scale independence of CN plays an important role. Fig. 7 shows results concerning $\langle CN\rangle(t)$.

Let us better analyse the results. The CN for the lower density "marching" setting is constantly zero. This is due to the fact that the velocity grid has many empty spaces, and the few points in which the rotor may be computed present the same local structure, and thus the same rotor (furthermore, the rotor field is actually zero everywhere). The high density case is more interesting. The maximum attained CN^M value is constant at ≈ 0.2, reaching slightly higher values at the times in which the flows start and finish crossing.

Since $CN^M(t)$ and $\langle CN\rangle(t)$ appear to be qualitatively similar, we may focus on density and maximum CN, and analyse the density, rotor and CN fields at times in which high ρ and CN values are attained. Let us define the *maximum density* as

$$\rho^M = \max_{t,r} \langle\rho\rangle_r(t), \tag{18}$$

where $\langle\rho\rangle_r(t)$ is the average density in the crossing area at time t and repetition r, and the *time and repetition of maximum density* as

$$\{\bar{t},\bar{r}\} = \operatorname*{argmax}_{t,r} \langle\rho\rangle_r(t). \tag{19}$$

Furthermore we may define the *highest* CN as

$$CN^{M*} = \max_{t,r} CN_r^M(t), \tag{20}$$

where $CN_r^M(t)$ is the maximum CN over all cells at time t and repetition r, and the *time and repetition of highest* CN as

$$\{t^*,r^*\} = \operatorname*{argmax}_{t,r} CN_r^M(t). \tag{21}$$

The "marching" velocity $\mathbf{v}$, density ρ, rotor $(\nabla\times\mathbf{v})_z$ and CN fields at $\{t^*,r^*\}$, the time and repetition in which the maximum (over cells) CN attains its highest value CN^{M*}, are shown in Fig. 8, while those at $\{\bar{t},\bar{r}\}$, the time and repetition of maximum density ρ^M, are shown in Fig. 9. At maximum density, the velocity patterns are regular over the central crossing area and in the corridors, and as a result in these areas we have low CN. CN reaches higher values in the "corners" where flows meet and separate. This effect is stronger when almost all pedestrians in the flows have passed the crossing area, as the velocity and rotor fields are less uniform.

An interesting result concerning the "zero body size" case is that the CN time evolution is basically independent of flow intensity. This is to be expected, since for non-interacting "particles" the increase in flow only changes the statistical sample, with no other effect on the vector fields. It is nevertheless important to see that the CN assessment metric is not "tricked" by the increased flow.

Fig. 10 (highest CN^{M*}) and Fig. 11 (maximum density ρ^M) concerning "zero body size" appear to be qualitatively similar to the marching ones, although they are more noisy. This is due to the fact that a constant velocity movement as the one of the "marching" pedestrians corresponds to the asymptotic state (in the zero noise limit) of the drifted walk performed by "zero body size" pedestrians.

For "finite body size" pedestrians, the crossing of the flows causes an actual congestion problem, due to the limited space and to the corresponding stopping/deviating behaviour. This is properly indicated by the higher (with respect to the "marching" and "zero body size" cases) value of CN, and by the fact that CN assumes higher values when a higher initial density is used. It is interesting to notice that when the $\rho = 2$ ped/m^2 initial condition is used, CN attains values ≈ 1. Fig. 12 shows the higher density setting $\mathbf{v}$, density, rotor and CN fields when CN^{M*} (which resulted to be as high as 1.26) is attained, while Fig. 13 shows the same fields when ρ^M is attained.

An interesting feature is that in the higher density setting, CN reaches (locally) extremely high values also when almost all pedestrians have passed and the density in the crossing area is decreasing. This is due to the situation depicted on the right in Fig. 4: some pedestrians are "dragged" in the wrong direction and high pressure/collision/congestion happens in the areas where they try to "go back". Around the bottom-right corner, such behaviour continues even when the majority of pedestrians has crossed (the occurrence of such a dynamics may be related to the simplicity in the pedestrians' local behaviour, and could be absent or reduced in actual pedestrians or in a more realistic model; anyway here we are not judging the pedestrian model but the ability of the assessment metric to recognise congestion and dangerous areas). The occurrence of such conditions is correctly identified by CN (Fig. 12).

5. CN In a crossing scenario experiment

We now present some data from controlled experiments in which 56 participants (28 for each flow) were asked to move in two different flows, using the same geometry as in the simulation settings (details concerning these experiments are described in (Zanlungo et al., 2023a); the experimental data are available at Feliciani et al., 2022). Although experiments and simulations share the same "crossing corridors" geometry, tracking in the experiments was performed only in the very proximity of the 3 by 3 m crossing area; and in order to minimise border effects we just cropped out the few data tracked outside the crossing space (the crossing area was then surrounded by empty cells when performing the CN computations). Results corresponding to two different initial conditions (1 and 2 ped/m^2) are shown (6 independent experiments were performed for each initial condition).

In Fig. 14, we report the time evolution of density in the crossing area $\langle\rho\rangle(t)$, maximum $CN^M(t)$ and average $\langle CN\rangle(t)$ over non-zero cells for both settings. Finally, for the 2 ped/m^2 condition, we show in Fig. 15 the $\mathbf{v}$, density, rotor and CN fields at the time and repetition in which CN^{M*} is attained, while those at the time and repetition in which maximum density ρ^M is attained are shown in Fig. 16.

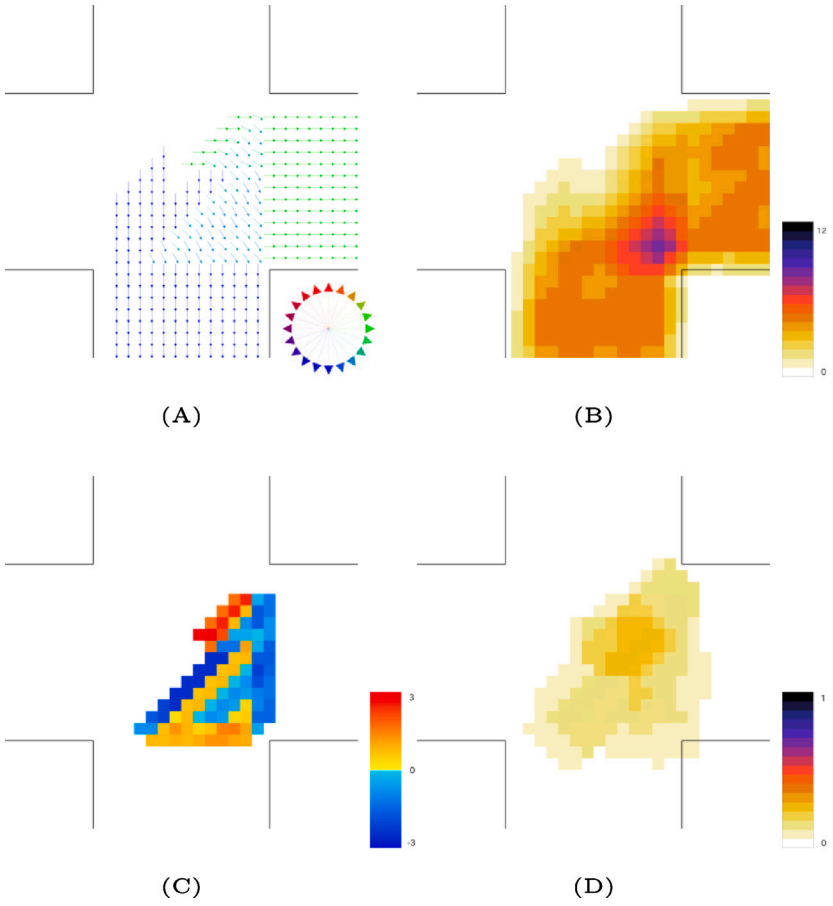

Fig. 8. Higher density "marching" pedestrians at the time in which the highest maximum CN, i.e. CN^{M*}, is attained ($CN^{M*} = 0.264$ at $t^* = [35, 37.5)$ s). (A): $\mathbf{v}$ field (m/s); (B): density ρ field (ped/m^2); (C): $(\nabla \times \mathbf{v})_z$ field (s^{-1}); (D): CN field. In the velocity field, the length of the arrow is proportional to the magnitude (full length $v > 0.5$ m/s), while the colour gives the orientation, as shown in the colour wheel legend. The density field is represented using a moving average over the Moore neighbourhood.

We may notice that CN assumes considerably lower values in the controlled experiment with respect to the "finite body size" simulation. Indeed, the potentially dangerous situation shown in Fig. 4, and to a smaller extent in Fig. 3 (pedestrians being pushed in the wrong corridor, or against walls), did not emerge for human subjects, due probably to a combination of smarter collision avoidance and smaller overall crowd size (furthermore, in the experimental settings we did not use actual walls, and corridors were delimited by ropes at leg height, see Zanlungo et al., 2023a for details). Nevertheless, the CN assessment metric appears to provide further information over what can be obtained by using just pedestrian density and flux, since higher values of CN are attained for human subjects with respect to "marching" and "zero body size" agents, although the initial density conditions are considerably lower.

Referring to the maximum value assumed by CN, we could thus say that $CN^M \approx 0.5$ appears to relate to an "intermediate" congestion state, in which the crowd is facing a "challenging" condition but it is not in a critically congested one. Such a value is also similar to the one reported for the data analysed by Feliciani and Nishinari (2018b). We nevertheless notice that the CN values attained in the controlled experiment with human participants are higher but not extremely higher than those attained, for example, in the "zero body size" simulation. The difference between the two situations can be assessed only when also the density is taken in consideration (namely, by considering how such relatively low CN values are attained by "zero body size" even at extremely high density). This should remind us of the dangers and limitations of using a single, although useful, indicator to assess the state of a crowd.

6. CN In other experimental settings and ecological environments

In the previous sections, theoretical aspects of the CN were presented and its properties were discussed taking a single geometry as example. In this section, we will consider a wider range of geometries and experimental conditions to better present the properties of the CN and also show applications in an ecological context in which the daily traffic of passengers in a train station is investigated.

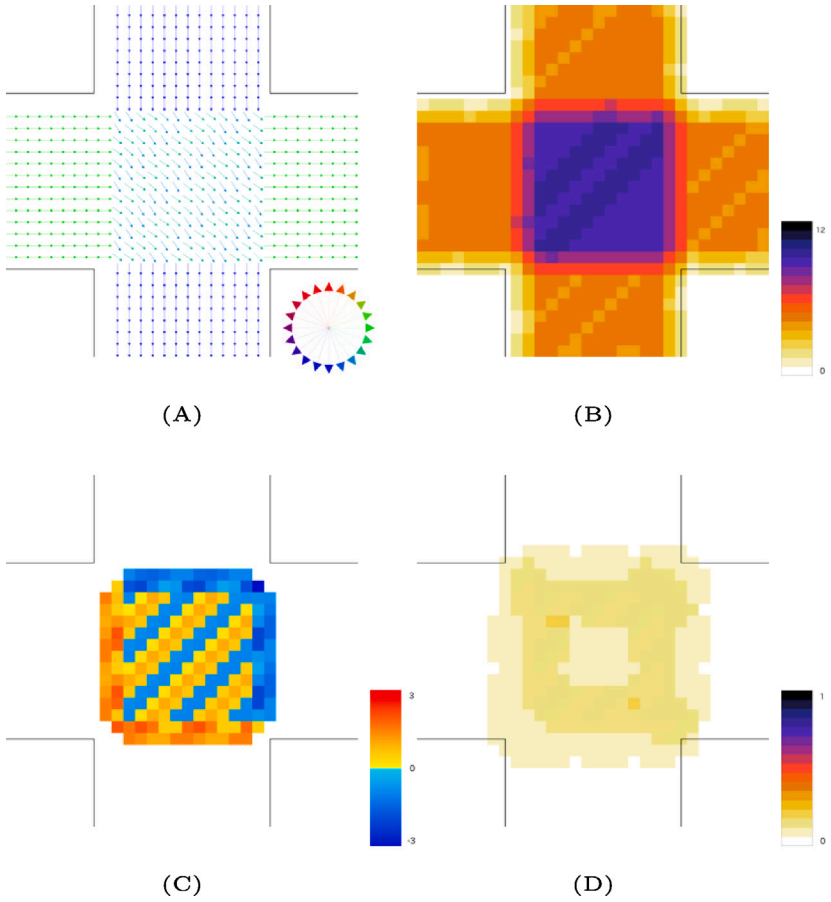

Fig. 9. Higher density "marching" pedestrians at the time in which the maximum density ρ^M is attained ($\rho^M = 8.78$ ped/m^2 at $\bar{t} = [27.5, 30)$ s). (A): $\mathbf{v}$ field (m/s); (B): density ρ field (ped/m^2); (C): $(\nabla \times \mathbf{v})_z$ field (s^{-1}); (D): CN field. In the velocity field, the length of the arrow is proportional to the magnitude (full length $v > 0.5$ m/s), while the colour gives the orientation, as shown in the colour wheel legend. The density field is represented using a moving average over the Moore neighbourhood.

Most of the works shown here were originally presented in other studies. So, readers interested in details are addressed to those studies. Nonetheless, we believe the results shown here should be sufficient to provide a practical understanding of applications of the CN in pedestrian facilities.

6.1. Pedestrian evacuation from a bottleneck

The bottleneck scenario is probably among the most studied in evacuation and pedestrian dynamics. Experiments were carried out by a large number of researchers also comparing the behaviour of people to that of animals or granular matter (Shiwakoti et al., 2019). Also, whether an obstacle placed in front of the exit will make evacuation faster or not has been the subject to a large debate and an agreement among researchers was not found. For the above reasons, we will start by presenting how the CN can help understanding the features found in bottlenecks. Fig. 17 shows the distribution of density and CN in a bottleneck scenario in presence and absence of an obstacle.

Some differences may be observed between the density and CN distributions, in particular concerning the location of the maximum value. In the case without the obstacle, high density values are observed close to the exit, where people are most packed. However, the maximum CN is found slightly in front of the bottleneck where multiple directions converge and motion becomes unstable. When the obstacle is introduced, maxima for both the density and CN distributions are found on the sides of the obstacles, although in this case the CN maxima tend to be closer to the exit than the density ones.

6.2. Dimensionality of motion and relationship with the CN

One of the characteristics of the CN lies in its ability to clearly distinguish the degree of self-organisation in crowds of people (as discussed using the "marching" scenario in the cross-flow setting, and below in Section 6.4). This aspect may be better

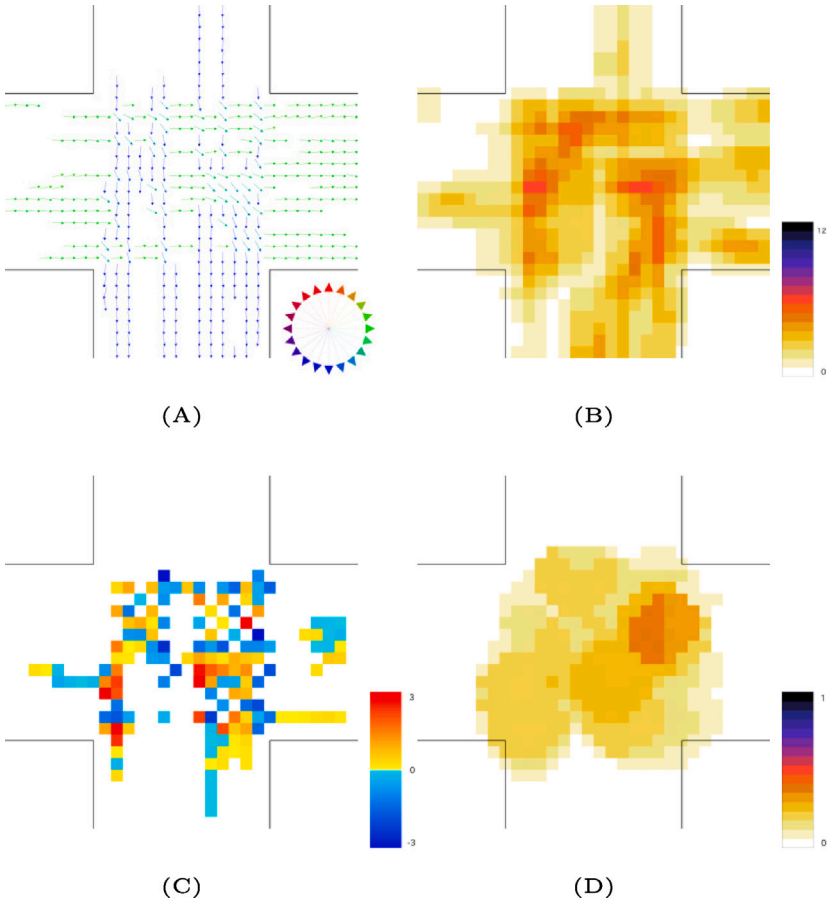

Fig. 10. Higher density "zero body size" pedestrians at the time in which CN^{M*} is attained ($CN^{M*} = 0.370$ at $t^* = [42.5, 45)$ s, $r^* = 6$). (A): $\mathbf{v}$ field (m/s); (B): density ρ field (ped/m^2); (C): $(\nabla \times \mathbf{v})_z$ field (s^{-1}); (D): CN field. In the velocity field, the length of the arrow is proportional to the magnitude (full length $v > 0.5$ m/s), while the colour gives the orientation, as shown in the colour wheel legend. The density field is represented using a moving average over the Moore neighbourhood.

investigated by considering experiments carried out having participants moving in multiple directions. The most simple case is the one represented by people moving in a corridor in a single direction. In such a case collision avoidance is not needed and regulating the distance with the person in front may be sufficient to keep a stable motion. On the other hand, the so-called bi-directional flow can be created by using the same corridor while having two groups of people moving in opposite directions. This creates non-trivial collision avoidance situations, typically leading to the deterioration of people flow (with respect to the uni-directional case) already at moderate densities (although this deterioration is limited by self-organisation phenomena, i.e. the splitting of the crowd in two spatially separated flows). The most complex scenario is the one represented by people moving randomly in a confined space. Several people may approach from different directions, making it difficult to predict which detour manoeuvre is the most appropriate to prevent collisions. We call the latter a "multi-directional" scenario.

Fig. 18 shows the CN evaluated at different densities for the three scenarios discussed above: uni-directional, bi-directional and multi-directional flows. As the graphs show, when the complexity of motion increases, higher values of CN are found for similar densities. Such an increase in CN is probably due to the detour manoeuvres needed to perform collision avoidance when different flows mix.

A comparison of the median CN value for the three scenarios at each density is shown in Fig. 19.

The profile observed in the multi-directional case may hint on the fact that a maximum CN is reached for asymptotically high densities. It is therefore possible to fit the multi-directional profile using an exponential function given as:

$$CN(\rho) = CN_{max} \cdot \left(1 - e^{-\kappa(\rho - \rho_0)}\right) \tag{22}$$

where κ is a fitting parameter, CN_{max} the maximum CN and ρ_0 the minimum density needed to take into account that CN cannot be computed at very low densities (or at least not by using the computational parameters defined in this work), since the density and velocity fields would present many empty cells. Specifically, a value of $CN_{max} = 0.523$ was found. The fact that such value is smaller than the theoretical maximum should not be surprising, since the data are relative to controlled experiments and people tend to

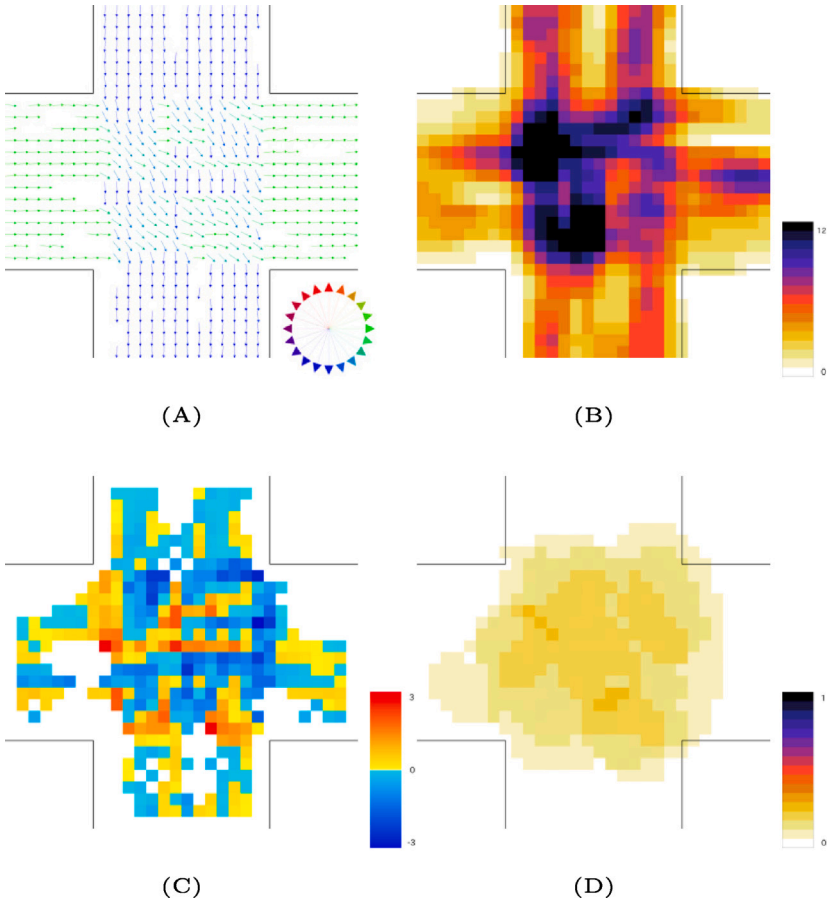

Fig. 11. Higher density "zero body size" pedestrians at the time in which the maximum density ρ^M is attained ($\rho^M = 9.5$ ped/m^2 at $\bar{t} = [25, 27.5)$ s, $\bar{r} = 6$). (A): $\mathbf{v}$ field (m/s); (B): density ρ field (ped/m^2); (C): $(\nabla \times \mathbf{v})_z$ field (s^{-1}); (D): CN field. In the velocity field, the length of the arrow is proportional to the magnitude (full length $v > 0.5$ m/s), while the colour gives the orientation, as shown in the colour wheel legend. The density field is represented using a moving average over the Moore neighbourhood.

slow down as density increases (i.e., they avoid, if possible, to behave in such a way to create dangerous conditions). Furthermore, a value of $\rho_0 = 0.426$ ped/m^2 was found, hinting that calculation of the CN is suitable for densities over 0.5 ped/m^2.

6.3. Application of the CN to an ecological context

We also present an application of the CN to a (real-world) ecological context in order to clarify its ability to provide information different from the one obtained by using only density, and in order to discus practical aspects related to its use for the purpose of crowd management. Here, trajectory data collected at the 2nd floor of JR Shinjuku station (Tokyo, Japan) are analysed. This floor is a concourse layer that connects to platforms and ticket gates, and its characteristics allow investigating the motion of a crowd in a complex structure. In the specific, the motion of people was collected over a 121 × 47 m^2 area managed by the East Japan Railway Company from 6:00 to 24:00 on December 15th 2020. Details on the layout, along with density and CN distributions, are presented in Fig. 20.

The most important feature in Fig. 20 is represented by the different shapes of the density and CN distributions, and in detail by the different location of maxima. More specifically, maximum density is found in corridors (the upper part of Fig. 20), a finding that can be explained considering the importance that these structures play by connecting several parts of the station. However, CN in corridors is relatively low, since, as explained above, motion is mostly limited to two directions. On the other hand, the maxima of the CN distributions are found in locations where different flows get mixed, leading more easily to collisions (or at least stronger collision avoidance).

We observe also that the maximum observed CN value is around 0.35, showing that in a real context, even when fairly crowded, values well below 1 are to be expected if the crowd is properly managed. On the other hand, it is worth mentioning that density is relatively low because values are averaged over 18 h, although much higher densities are observed during peak hours.

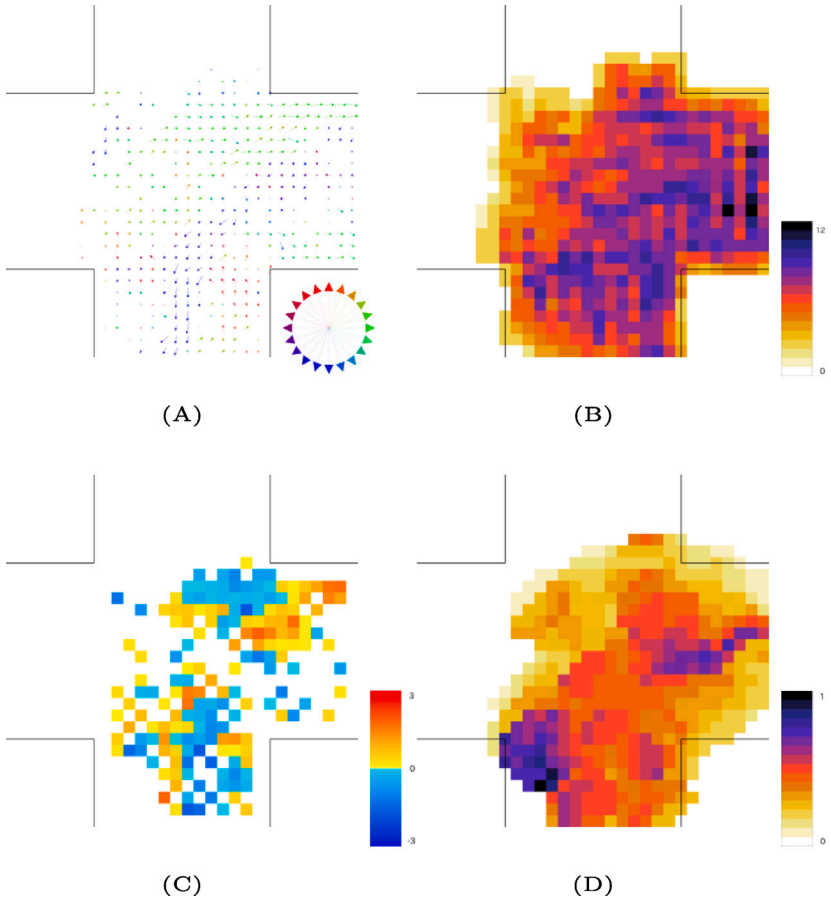

Fig. 12. Higher density "finite body size" pedestrians at the time in which CN^{M*} is attained ($CN^{M*} = 1.258$ at $t^* = [55, 57.5)$ s, $r^* = 9$). (A): $\mathbf{v}$ field (m/s); (B): density ρ field (ped/m^2); (C): $(\nabla \times \mathbf{v})_z$ field (s^{-1}); (D): CN field. In the velocity field, the length of the arrow is proportional to the magnitude (full length $v > 0.5$ m/s), while the colour gives the orientation, as shown in the colour wheel legend. The density field is represented using a moving average over the Moore neighbourhood.

6.4. CN In a transient context (bi-directional flow in a ring)

So far, only plots showing the spatial distribution of density and CN were presented. However, the CN can also be used to detect changes in the collective organisation of crowds, regardless of density or speed.[7] In this section we discuss an experiment in which participants are asked to walk in opposite directions a circular path (a "ring" creating periodic boundary conditions and thus facilitating the emergence of self-organisation).

As shown in Fig. 21, participants were initially randomly distributed over the course and different "structures" (small groups of co-moving people) rapidly formed as they walked in opposite directions. In one case, a stable configuration having two distinguished lanes emerged, with the transition to such a self-organised structure clearly depicted by a sudden drop in CN. In another condition, a sort of spiral configuration was formed with groups constantly moving from the inner to the outer portion and creating conflict situations. In this case, the CN constantly oscillates taking higher values during conflict situations and decreasing when lanes are almost non-interacting (separated).

This example clearly shows a difference between the information provided by the CN with respect to an analysis based only on speed and density. Indeed, in this scenario, density is constant by definition and speed presents only slight changes. On the other hand, variations in CN appear to represent the emergence of collective organisation within the crowd, showing the potential of CN in identifying risky locations in a real context.

[7] This aspect was also partially considered while discussing the cross-flow, but mainly from a theoretical perspective.

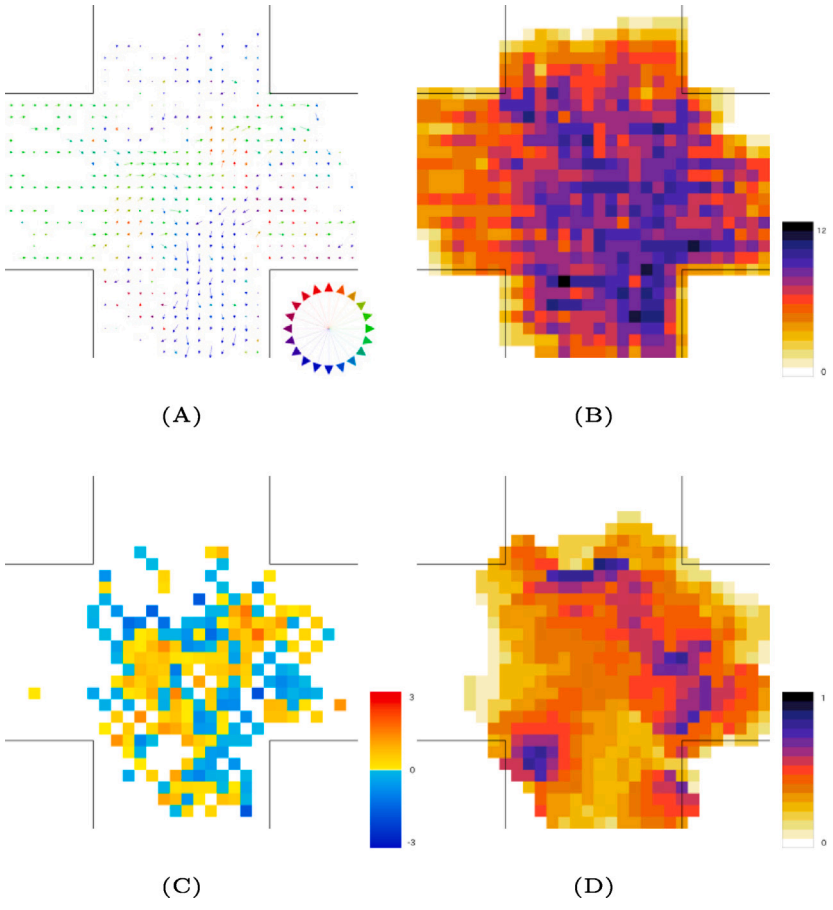

Fig. 13. Higher density "finite body size" pedestrians at the time in which the maximum density ρ^M is attained ($\rho^M = 8.79$ ped/m^2 at $\bar{t} = [37.5, 40)$ s, $\bar{r} = 4$). (A): **v** field (m/s); (B): density ρ field (ped/m^2); (C): $(\nabla \times \mathbf{v})_z$ field (s^{-1}); (D): CN field. In the velocity field, the length of the arrow is proportional to the magnitude (full length $v > 0.5$ m/s), while the colour gives the orientation, as shown in the colour wheel legend. The density field is represented using a moving average over the Moore neighbourhood.

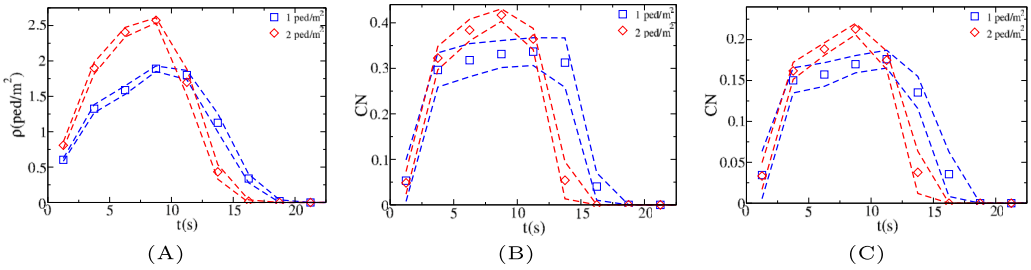

Fig. 14. (A) Density in the crossing area $\langle \rho \rangle(t)$; (B) maximum $CN^M(t)$; and (C) average $\langle CN \rangle(t)$ over non-zero cells; as a function of time in the controlled experiments with human subjects. Observables are averaged over 6 different initial conditions and on time intervals of 2.5 s. Dashed lines provide standard error bars.

7. Conclusions

The Congestion Level CL is a recently introduced metric to assess the emergence and presence of potentially dangerous or at least problematic conditions in a pedestrian crowd. In this work, we investigated the theoretical foundations of the CL definition, and suggested an alternative metric, the Congestion Number CN. The CN is a pure number with no explicit dependence on computational parameters, and has a straightforward interpretation ($CN \ll 1$ corresponding to not congested state, $CN \approx 1$ corresponding to extreme congestion).

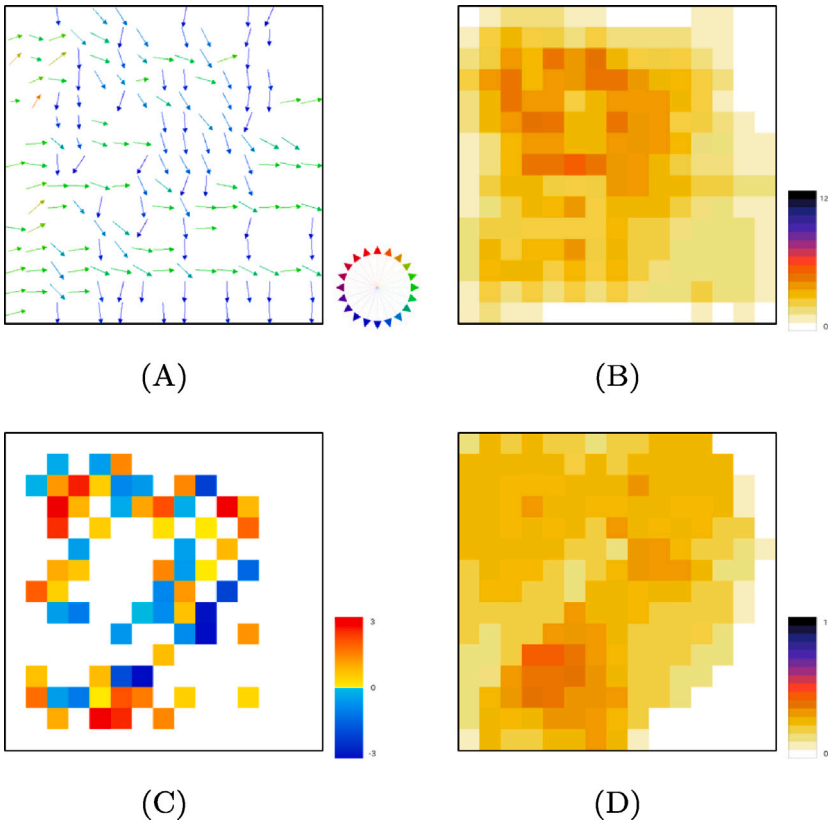

Fig. 15. Pedestrians in the 2 ped/m^2 condition controlled experiments at the time CN^{M*} is attained ($CN^{M*} = 0.451$ at $t^* = [7.5, 10)$ s, $r^* = 1$). (A): $\mathbf{v}$ field (m/s); (B): density ρ field (ped/m^2); (C): $(\nabla \times \mathbf{v})_z$ field (s^{-1}); (D): CN field. In the velocity field, the length of the arrow is proportional to the magnitude (full length $v > 0.5$ m/s), while the colour gives the orientation, as shown in the colour wheel legend. The density field is represented using a moving average over the Moore neighbourhood.

To better clarify the main features of the CN, we initially focused on cross-flow scenarios, which were deemed to be complex enough to need an analysis using information beyond the one provided just by density and flow values, but still simple enough to be used to investigate the properties of a new crowd indicator.

By computing CN values for simulations using agents that, either being externally controlled with a pre-assigned velocity, or lacking actual body size, did not need to perform any collision avoidance behaviour, we verified that the proposed assessment metric is able to detect the lack of any actual congestion problem even in presence of high density and flux. On the other hand, by using agents that had an actual finite body size and (possibly relatively inefficient) collision avoidance behaviour, we verified the occurrence of $CN \approx 1$ conditions when pedestrians appeared to be unable to freely move towards their preferred destination. Finally, the analysis of an experiment using human subjects in a similar setting showed the occurrence of intermediate CN values, which appeared to reflect the actual state of the crowd (presence of a still manageable congestion problem).

We then analysed different scenarios, such as bottlenecks, uni-, bi- and multi-directional settings, a real-world railway station, and a bi-directional flow over a loop. The last two scenarios were particularly interesting. The study of the movement of pedestrians in the Shinjuku railway station (Section 6.3) shows that, even when considering a real-world setting, the proposed CN indicator provides information qualitatively different from the one that can be derived from density patterns. The study of the movement of pedestrians over a loop (Section 6.4) shows that, at least in the proposed controlled scenario, such information is extremely valuable, as changes in the self-organisation state of the crowd were clearly identified by corresponding changes in the CN value, although density and speed values were unchanged.

Since the concept of CN has just been proposed, it is obviously impossible at the current stage to provide a clear correlation between the observed values of such indicator and the "level of danger" of an actual real-world (or even controlled) crowd, and with this work we obviously do not propose to abruptly replace well-studied crowd metrics with the proposed indicator, nor we propose a clear "threshold" to differentiate between safe and dangerous states. Indeed, it is unrealistic to believe that a single number may completely define the state of a complex system like a crowd, and indeed in a few points of the manuscript we hint to the necessity of taking in account other observables, such as density.

Nevertheless, we hope that the findings of this manuscript suggest that the proposed indicator is of possible value, and will stimulate further studies of its properties and applications.

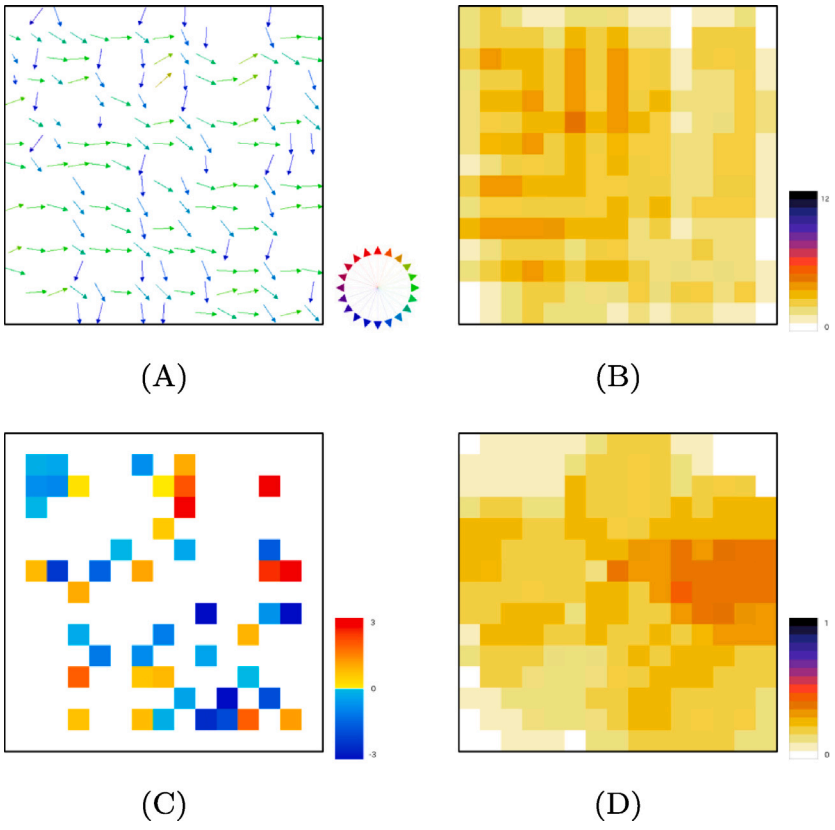

Fig. 16. Pedestrians in the 2 ped/m^2 condition controlled experiments at the time in which the maximum density ρ^M is attained ($\rho^M = 2.65$ ped/m^2 at $\bar{t} = [7.5, 10)$ s, $\bar{r} = 6$). (A): $\mathbf{v}$ field (m/s); (B): density ρ field (ped/m^2); (C): $(\nabla \times \mathbf{v})_z$ field (s^{-1}); (D): CN field. In the velocity field, the length of the arrow is proportional to the magnitude (full length $v > 0.5$ m/s), while the colour gives the orientation, as shown in the colour wheel legend. The density field is represented using a moving average over the Moore neighbourhood.

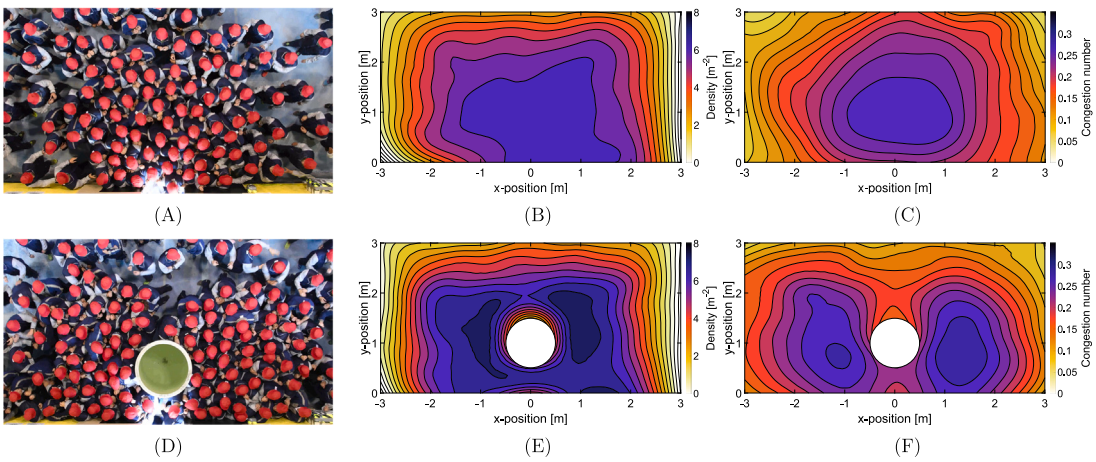

Fig. 17. Average density and CN for evacuation drills through a single bottleneck without ((A): experimental setting; (B): density; (C): CN) and with ((D): experimental setting; (E): density; (F): CN) an obstacle. The exit (bottleneck) has a width of 75 cm and is located in the middle of the x-axis. Distributions are computed over multiple trials performed under the same experimental condition. Details on the analysis and on the experiments can be found in Feliciani et al. (2020a).

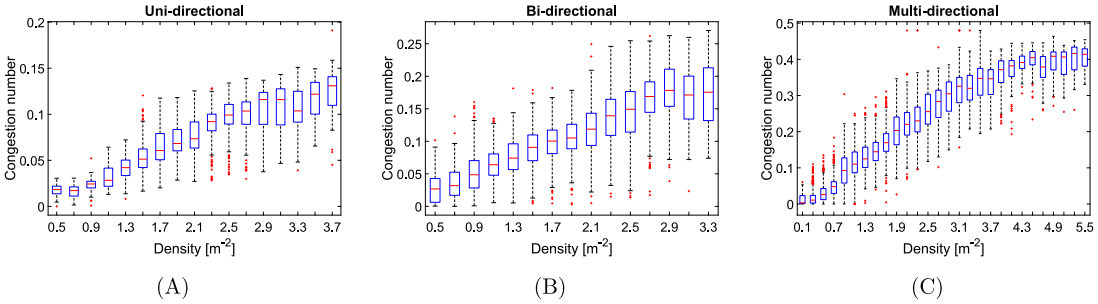

Fig. 18. CN shown as a function of density for controlled experiments reproducing different types of crowd motion. Data from several experiments concerning (A) uni-directional, (B) bi-directional and (C) multi-directional flows are examined and results summarised in bins having a size of 0.2 ped/m^2. For each bin, a box representation is used, with the central mark being the median and the bottom and top edges indicating the 25th and 75th percentiles, respectively. Extreme points are represented using whiskers and outliers shown in red markers. Details on the experiments are given by Zhang et al. (2012) and Feliciani and Nishinari (2018b).

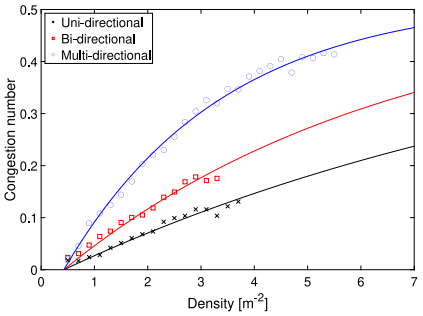

Fig. 19. Relation between CN (median values from Fig. 18) and density for crowd motion under different degrees of freedom. The multi-directional case is used to calibrate CN_{max} and ρ_0, which are later used to fit the uni-directional and bi-directional cases.

Finally, although we often show graphs concerning the time variation of CN, only spatial derivatives (i.e., no time derivatives) where included in its definition. As time variation is of clear importance in the assessment of instabilities in a crowd, both the inclusion of time variation in the very definition of CN, and the importance of time variation of CN as defined in this work, should be the subject of future studies.

CRediT authorship contribution statement

Francesco Zanlungo: Conceptualization, Formal analysis, Methodology, Software, Visualization, Writing – original draft, Writing – review & editing. **Claudio Feliciani:** Conceptualization, Data curation, Investigation, Writing – original draft, Writing – review & editing. **Zeynep Yücel:** Visualization, Writing – review & editing. **Xiaolu Jia:** Data curation, Investigation. **Katsuhiro Nishinari:** Conceptualization, Funding acquisition. **Takayuki Kanda:** Funding acquisition, Writing – review & editing.

Declaration of competing interest

The authors declare that they have no known competing financial interests or personal relationships that could have appeared to influence the work reported in this paper.

Acknowledgements

Funding

This research work was in part supported by: JSPS, Japan KAKENHI Grant Number JP18H04121, JSPS, Japan KAKENHI Grant Number JP20K14992, JSPS, Japan KAKENHI Grant Number JP21K14377, JST-Mirai Programme, Japan Grant Number JPMJMI17D4 and JPMJMI20D1. In addition, the authors would like to express gratitude to JR East Railway Company for providing the Shinjuku Station data.

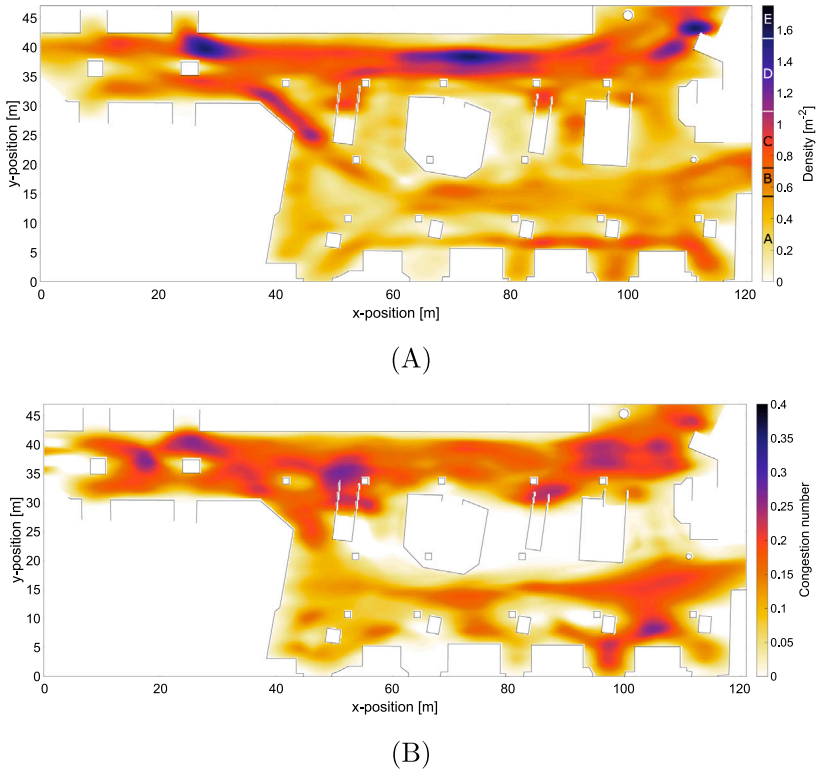

Fig. 20. (A) Average density and (B) CN during a 18 h data collection period on the 2nd floor of JR Shinjuku station (Tokyo, Japan). Results were smoothed using the LOWESS smoothing method of Mathworks (2022) to reduce sensing noise and create a more continuous representation for both density and CN. The pedestrian trajectories used for calculation were obtained using Velodyne VLP-16 3D LiDAR sensors installed in 11 locations to cover the majority of the concourse layer. Boundaries of the concourse are depicted by black lines. The colour bar for the density distributions reports also the values (letters from A to E) associated with different "Level-Of-Service" (flat walkways) densities.

Data and software availability

The data analysis software, along with simulated pedestrian data, is available at Zanlungo (2020). The human subject experiment data is available at Feliciani et al. (2022).

Appendix A. Comments on the choice of the cross-flow scenario

We want our indicator to be able to identify a tendency, manifest at the macroscopic crowd level, of pedestrians to deviate from their preferred path (i.e., at the crowd level, from the crowd's "natural flow"), because such deviations are expected to "congest" or "disrupt" the flow of the crowd. Since preferred paths are in principle unknown, we expect this tendency to be expressed through local "irregularities" in the velocity field, irregularities that, in the approach of this work, are defined through the variation in the magnitude of the velocity rotor (see Section 3 for the formal definition). We thus wanted to identify a scenario that was simple enough to allow a systematic treatment from theoretical, simulation and experimental view-points, but complex enough to cause the aforementioned disruption of the crowd's flow. We believe the cross-flow (see Sections 4, 5 for procedural definitions) to be such a scenario. Indeed, while in most systematically studied scenarios, such as uni-directional flow, bottleneck and evacuation from an exit, all the pedestrians in the crowd roughly share the same goal,[8] in a cross-flow pedestrians with clearly different goals need to share the same space (the crossing area) at the same time. The bi-directional flow could seem to be a possible alternative, but in such a scenario a good level of separation between the two flows can be attained by using a simple self-organising rule (e.g., "walk on the left side"; such rules are actually known to be strongly followed at least in some real-world environments Zanlungo et al., 2012). On the other hand, while also the flow in a crossing area can be optimised through a "stripe formation rule" (see Sections Section 4, 5), such a rule requires a high level of coordination between pedestrians and will necessarily be only partially attained by self-organisation. For these reasons, we expect the "flow disruption" that we want to analyse in this work to naturally arise in the cross-flow scenario.

[8] This is partially true also for a multi-exit scenario, as the highest densities and flows are usually attained in the proximity of a given exit.

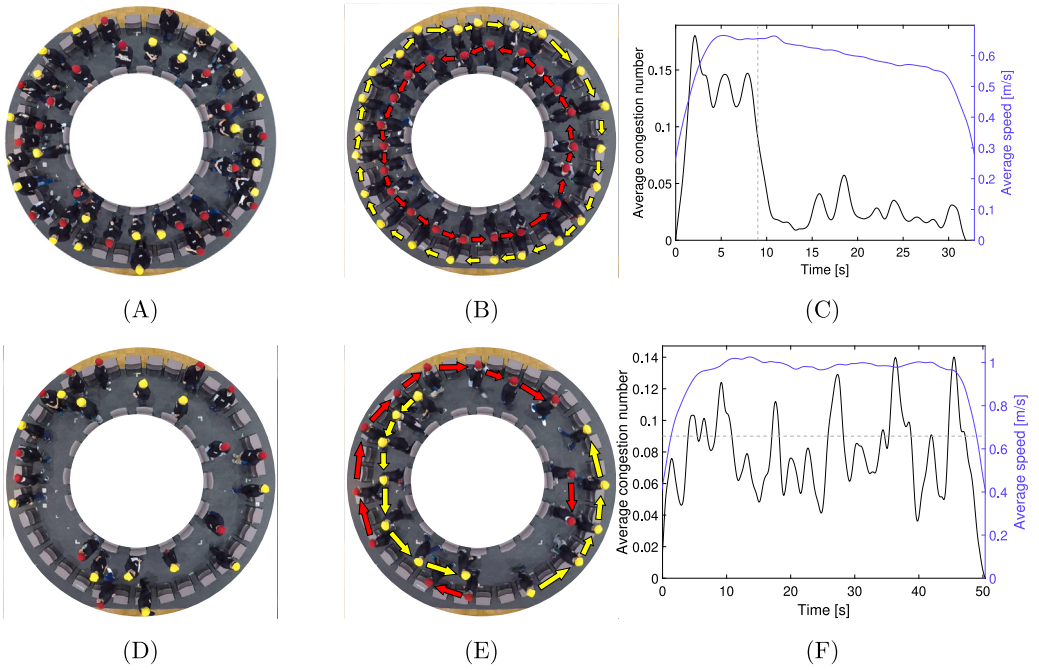

Fig. 21. Experimental setting, average speed and CN for a bi-directional flow in a ring. (A) reports the initial condition of an experiment repetition in which the crowd reaches a high level of self-organisation towards the end of the experiment, shown in (B). The corresponding speed (in blue) and CN (black) time evolutions are shown in (C). On the other hand, (D) (initial condition), (E) (condition towards the end of the experiment) and (F) (speed and CN plots) correspond to a repetition that attained a lower level of self-organisation. In both cases, people with red and yellow caps walk in opposite directions (clockwise and counter-clockwise). In (C) the transition into a stable configuration is shown using a dotted vertical line. In (F) the CN during the aforementioned transition (the intersection between the curve in (C) and the dotted line, corresponding to 0.09) is reported using a horizontal line to make comparison easier. Details on experimental conditions are given by Feliciani and Nishinari (2018b).

Appendix B. Comments on the motivation of this work and on the use of the term "congestion"

The purpose of this work is to improve the definition of the Congestion Level by introducing a dimensionless "Congestion Number" and to elucidate its main properties. The Congestion Level and the work defining it (Feliciani and Nishinari, 2018b) are taken as a starting point, and in this work we do not try to justify the introduction of CL. Nevertheless, it may be useful to provide a few comments on its motivation and on the choice of the name.

The fundamental idea is to identify possibly "problematic" conditions in a pedestrian crowd, and the assumption is that such conditions may be related to a pedestrian flow that abruptly changes in time and space. The obvious parallel in fluid dynamics is the emergence of a turbulent state. Nevertheless, as discussed in Section 2, defining a velocity field for a crowd involves problems related to the characteristic scales of crowd dynamics, that do not allow to properly perform a "continuous limit" in space and time. For these reasons, we tried to define a relatively simple "index" that could identify the presence of a "turbulent flow" just through a rough definition of a velocity vector field over a spatial lattice with a grid size comparable to human size, and without taking in account time derivatives.[9] We were thus inspired by the presence, in turbulent flows, of many eddies and vortices, and we considered that the emergence of a similar state in the crowd could be tested by measuring the rotor of the velocity field and its variation in space.

Concerning the name "congestion", it was intended as a proxy for a state in which the crowd is "not normally flowing", and thus is getting "congested". Although some of the ideas behind the CL and CN concept are inspired by concepts in fluid dynamics, we prefer not to use the term "turbulence", as we do not claim this work to be a contribution to the study of turbulence in fluid dynamics. A possible alternative term could be "crowd flow disruption", by which we mean a tendency to deviate from preferred paths due to the state of the crowd. Nevertheless, in this work we stick to the name "congestion" in order to create a clear connection with the previous work (Feliciani and Nishinari, 2018b) and with other crowd research studies that used the CL concept, such as Feliciani et al. (2018), Fujita et al. (2019), Feliciani and Nishinari (2020), Feliciani et al. (2020b), Ye et al. (2020, 2021) and Hosseini et al. (2021).

[9] The choice not to take in consideration time derivatives, at least in this first approach, is mainly due to two considerations: first of all, although it appeared to us that the problem has a clear minimum spatial scale (human body size), we could not identify a corresponding "natural" time scale; furthermore, a time scale has to be introduced in our computations to obtain a relatively smooth velocity field, see the discussion in Appendix C, over the chosen grid, and thus the computational time scale appears to be "subordinate" to the spatial one, making the meaning of time derivatives harder to interpret.

Appendix C. Choice of computational parameters

Three computational parameters need to be defined in order to compute the CN, namely the size of the grid R, the averaging time Δt and the size of the ROI, L. The first two parameters are actually needed to define the very velocity field (as the average of velocities falling in the 2+1 dimensional R-by-R-by-Δt volume), while R is used also to compute (at each time $k\Delta t$) the rotor field, and L is needed to compute the CN proper. All the computations in this work have been based on the definitions by Feliciani and Nishinari (2018b) and Feliciani and Nishinari (2020), although a theoretical justification for the choice of R and L has been provided (see in particular Appendix D).

With respect to CL, CN has the advantage of not depending explicitly on these parameters (CL has an explicit dependence on R), and thus it could seem possible to define the optimal parameters as those for which we have a convergence in the CN value. Nevertheless, after a second thought, it is clear that such an analysis is not trivial. Although the theoretical definition of CN is based on assuming the existence of a continuous velocity field, such a rigorous continuous approach is possible only using scales much larger than those at which interesting congestion phenomena appear (see Lautrup, 2011), and thus convergence is expected for parameter values considerably larger than those proposed by Feliciani and Nishinari (2018b) and Feliciani and Nishinari (2020). Furthermore, the three parameters are inherently different from a dimensional view point (R being a continuous length, L a multiple of R, and Δt a time).

We may nevertheless try to perform a quantitative analysis of parameter stability by assuming the choice of Feliciani and Nishinari (2018b) and Feliciani and Nishinari (2020) as a starting point, defining a grid in parameter space over a scale compatible with such a choice, and analyse the stability over such grid.

Namely, we may investigate the value attained by the maximum over time of CN, averaged over the set of all repetitions $\{r\}$ (e.g., the peaks of Fig. 6), or

$$M = \langle \max_t CN_r^M(t) \rangle_{\{r\}}, \tag{C.1}$$

for the "finite body size" simulation data by changing the parameters in the following ranges: $R = i\,0.05$ m, $L = j\,R$, $\Delta t = k\,0.5$ s, with $i, j, k = 1, \ldots, 10$. Writing the explicit dependence of M over $\{i, j, k\}$ through the notation $M_{i,j,k}$ we may then compute the magnitude of the "gradient"

$$\begin{aligned} \Delta_x &\equiv M_{i+1,j,k} - M_{i-1,j,k}, \\ \Delta_y &\equiv M_{i,j+1,k} - M_{i,j-1,k}, \\ \Delta_z &\equiv M_{i,j,k+1} - M_{i,j,k-1}, \\ G_{i,j,k} &\equiv \sqrt{\Delta_x^2 + \Delta_y^2 + \Delta_z^2}. \end{aligned} \tag{C.2}$$

Figs. 22–24 show the results. In the $\rho = 1$ ped/m^2 initial condition setting (Fig. 22) the highest maximum CN, M (Eq. (C.1)), converges to a stable value for $R \gtrsim 0.3$, $L \gtrsim 5R$, $\Delta t \gtrsim 2.5$, values comparable, although higher, than those used in this work. It has nevertheless to be considered that choosing a ROI with a diameter ≈ 3 m corresponds to covering almost the whole crossing area with a single ROI, and thus losing local information. The proposed values (detailed in Fig. 23) appear then as a compromise to retain local information, while cutting off the parameter area with strong instability (high gradient).

As density grows, convergence is faster and already almost attained around the proposed parameters (Fig. 24). Indeed, an analysis of the CN values for the minimum gradient points shows that they are very similar to those found using the proposed parameters. Namely, defining

$$\{i_m, j_m, k_m\} = \operatorname*{argmin}_{i,j,k} G_{i,j,k}, \tag{C.3}$$

we see the highest maximum CN value for the minimum gradient point is $M_{i_m,j_m,k_m} \approx 0.58$ for the $\rho = 1$ ped/m^2 initial condition at $R = 0.35$ m, $L = 9R$, $\Delta t = 3.5$ s; while for the $\rho = 2$ ped/m^2 initial condition we have $M_{i_m,j_m,k_m} \approx 0.9$ at $R = 0.35$ m, $L = 7R$, $\Delta t = 4$ s. A comparison with Fig. 4 shows that using the proposed parameter values CN has already attained a value compatible to the one at "convergence" (minimum gradient).

Appendix D. Toy models of high CN settings

D.1. Discrete approach

Let us study some settings that correspond to very high CN values, first using a derivation more closely related to the numerical nature of the computation. Such a "discrete derivation" has the following interesting properties:

1. does not rely on a fictitious continuous field defined at a scale much smaller than R,
2. clearly explains the relation between L and R,
3. clearly explains the role of the approximation $\langle v \rangle_{R(\mathbf{x})} \approx \langle v \rangle_{D_R}$ in our derivation,
4. explains the role of numerical approximations (e.g. choice of integration/differentiation schemes).

In Appendix D.2, we take the opposite approach, i.e., perform all computations on a microscopic, continuous velocity field.

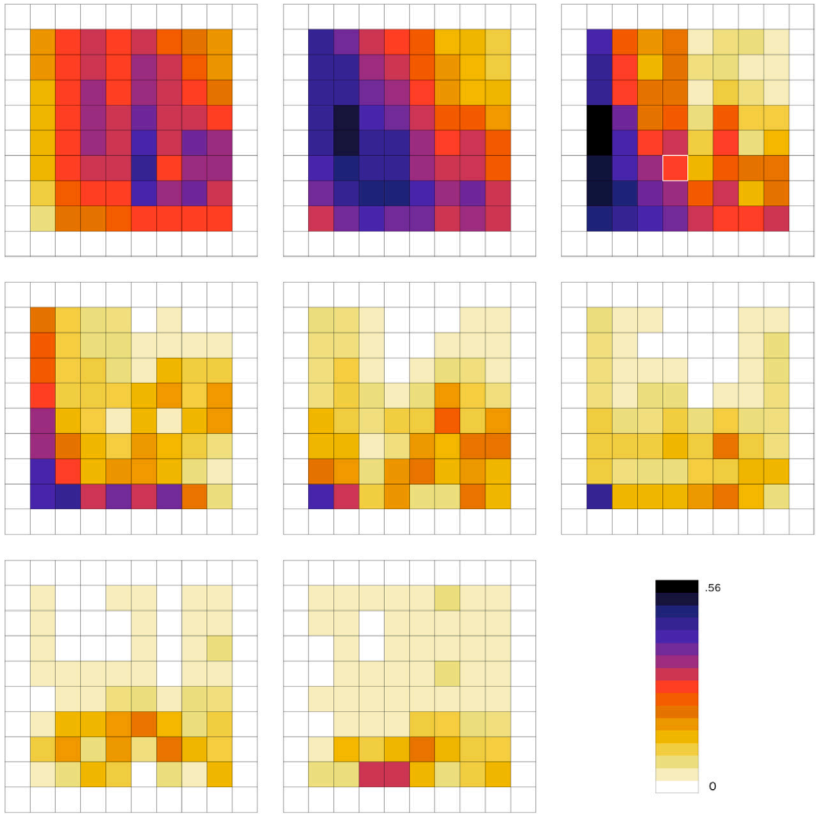

Fig. 22. Gradient $G_{i,j,k}$ as a function of Δt (abscissa axis) and L (ordinate axis, refer to Fig. 23 for details) for values of $R = i\,0.05$ m, $i = 2, \ldots, 9$ (growing from left to right, top to bottom). "finite body size" simulation data with $\rho = 1$ ped/m^2 initial condition.

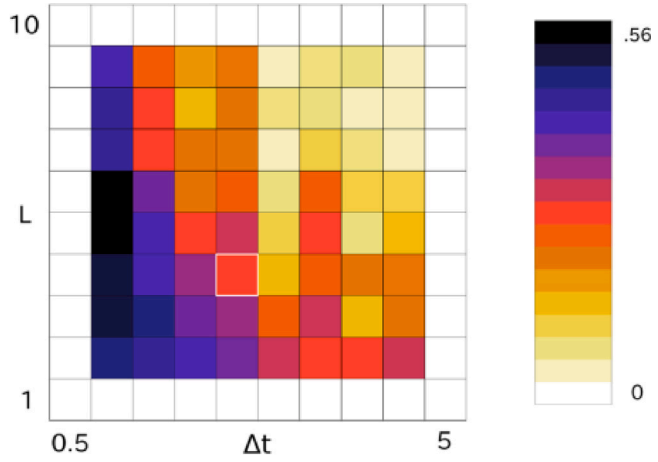

Fig. 23. Gradient $G_{i,j,k}$ as a function of Δt and L for $R = 0.2$ m. The value $L = 4$, $\Delta t = 2.5$, close to the one used in the rest of the work ($R = 0.2$ m, $L = 3.5$, $\Delta t = 2.5$) is highlighted by white borders. "finite body size" simulation data with $\rho = 1$ ped/m^2 initial condition.

D.1.1. Separated, random constant velocity

The discrete equivalent of two opposite maximally rotating fields located at a close distance can be realised on the grid shown in Fig. 25 (A). The maximum rotor value occurs in the cell 2, while the minimum occurs in cell 3. We are going to compute CN in cell 1, which is in the middle of the two flows (and separated from them). If the cells have size R, the distance between cells 2 and 3 is $L = 4R$. The vector field has magnitude v in the direction given by the arrows, and we assume it to have constant magnitude v but random direction on all other cells. In such a way, regardless of the choice of the ROI, the value of $\langle v \rangle_{\mathrm{ROI}}$ is going to be v.

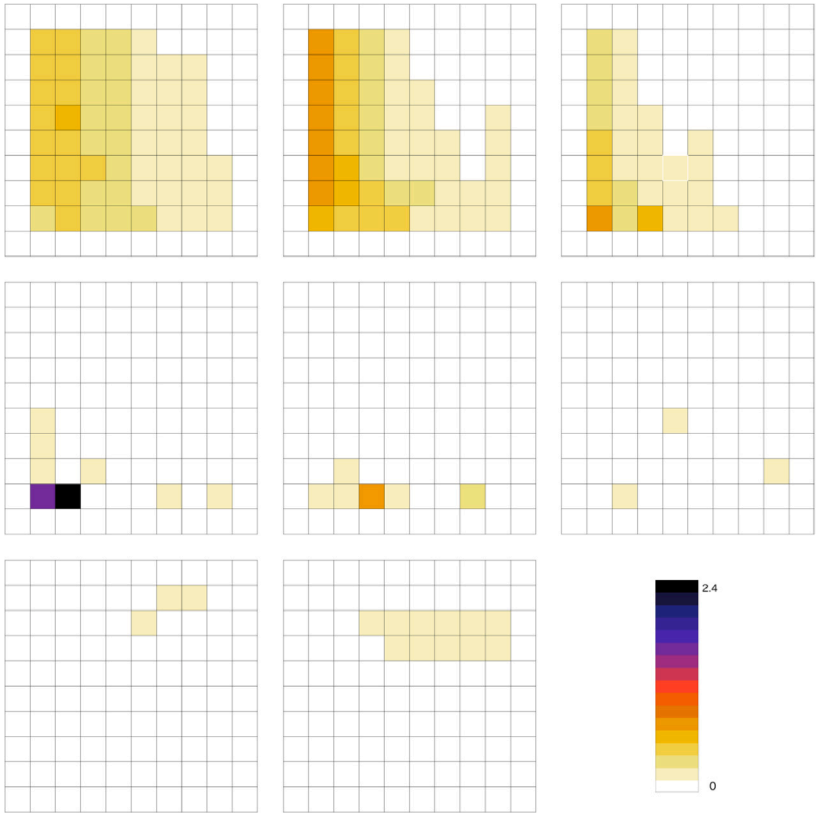

Fig. 24. Gradient $G_{i,j,k}$ as a function of Δt (abscissa axis) and L (ordinate axis, refer to Fig. 23 for details) for values of $R = i\,0.05$ m, $i = 2, \ldots, 9$ (growing from left to right, top to bottom). "finite body size" simulation data with $\rho = 2$ ped/m^2 initial condition.

We recall that

$$(\nabla \times \mathbf{v})_z = \partial_x v_y - \partial_y v_x. \tag{D.1}$$

Using the most trivial numerical differentiation scheme, in cell 2 we have

$$(\nabla \times \mathbf{v})_z = \frac{2v}{2R} - (-\frac{2v}{2R}) = \frac{2v}{R}, \tag{D.2}$$

while obviously in 3 we have the opposite value, so that

$$\max(\nabla \times \mathbf{v})_z - \min(\nabla \times \mathbf{v})_z = \frac{4v}{R}, \tag{D.3}$$

and

$$CN = \frac{4v}{R}\frac{R}{6v} = \frac{2}{3}. \tag{D.4}$$

The reason we obtained a value different from 1 is due to the difference between the values of the average velocity in the continuous model used to define CN and in the discrete model. Anyway, higher values of CN are possible, as shown next.

D.1.2. Separated, negligible velocity outside flows

Let us now go back to Fig. 25, but this time we may assume that velocity is *almost* 0 (i.e., $\ll v$) where arrows are lacking (including cells 1, 2 and 3). This choice of having a lot of cells with very low velocity is due to the attempt of keeping $\langle v \rangle$ as small as possible, and thus CN as large as possible. It should be noticed that an empty cell is, from the crowd dynamics viewpoint, extremely different from a non-empty cell with a low velocity, and indeed (Feliciani and Nishinari, 2018b) remind us to compute average velocities using only occupied cells. Anyway, in the computations below, the cells without arrows may be considered with such a small velocity (e.g., $10^{-3}v$) that their contribution to averages and rotors is simply ignored (from an actual crowd dynamics viewpoint, obviously, this is quite unrealistic).

The value of $\langle v \rangle_{\mathrm{ROI}}$ depends now strongly on the definition of the ROI. It seems obvious that the ROI should include all non-zero cells, so that its "diameter" (maximum distance between two included cells) has to be at least $7R$, which is exactly the value empirically proposed by Feliciani and Nishinari (2018b). The actual choice of the ROI depends then on the definition of the distance on the grid. We propose here 3 schemes:

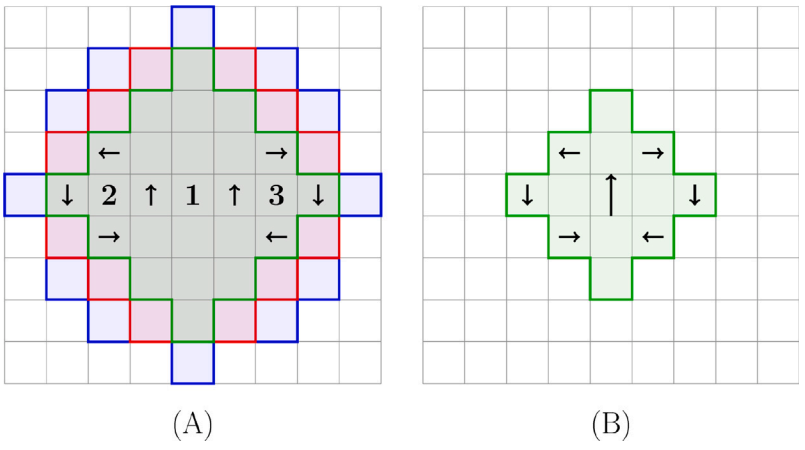

Fig. 25. (A): separated flows. MM scheme boundary in green, OE scheme boundary in red, ME scheme boundary in blue. (B): overlapping flows.

1. Manhattan distance: only cells at a Manhattan distance $d_M = |dx| + |dy| \leq 3$ are included. This includes exactly $N_{\mathrm{ROI}} = 25$ cells, as shown in Fig. 25 (A) (Minimum Manhattan scheme, or MM).
2. The original scheme proposed by Feliciani and Nishinari (2018b), i.e., including, since the diameter of the ROI is 7, all cells that have a Euclidean distance between their centres $d_E \leq 7R/2$. This includes 37 cells (Original Euclidean scheme, or OE).
3. As above, using Euclidean distance but, since the distance between cells 2 and 3 is $L = 4R$, requiring $d_E \leq 4R$. This includes 49 cells (Maximum Euclidean scheme, or ME).

Since only 8 cells have non-zero v, the value of $\langle v \rangle$ would be 8 v/N_{ROI}, and thus

$$CN = \frac{N_{\mathrm{ROI}}}{8v}\frac{4v}{R}\frac{R}{6} = \frac{N_{\mathrm{ROI}}}{12}, \tag{D.5}$$

which gives a value higher than 4 in the ME scheme. It seems anyway reasonable that these extremely artificial conditions may not occur in the real world and values of $CN \approx 1$ should already be considered as extremely high.

In such a setting, the same values are found in case we use a single maximally rotating field, e.g. in the centre of the cell, since the numerator is decreased by a factor two, but also the denominator is equally decreased (the number of non-empty cells would be 4). These results may be puzzling, but, again, we should remember that CL has been proposed by Feliciani and Nishinari (2018b) to deal with actual crowds, and not with our handpicked situations. Furthermore, "empty cells" in our settings should actually represent occupied cells with very low velocity (packed crowd), and it is clear that having a strongly rotational movement inside a packed, almost non-moving crowd, should be a hint of a potentially very dangerous situation in an actual crowd.

D.1.3. Overlapping, random constant velocity

If in Fig. 25 we displace both maximally rotating fields by one cell towards the centre (Fig. 25 (B)) we get a non-zero field in 1 ($\mathbf{v} = (0, 2v)$). In this case, the absolute value of the maximum and minimim rotor is

$$|(\nabla \times \mathbf{v})_z| = \frac{3v}{2R} - (-\frac{2v}{2R}) = \frac{5v}{2R}. \tag{D.6}$$

If the velocity in the other cells has constant magnitude v we get

$$CN = \frac{5v}{R}\frac{R}{6v} = \frac{5}{6}. \tag{D.7}$$

D.1.4. Overlapping, negligible velocity outside flows

Assuming negligible velocity outside the flows, we now get, by having just 7 "non-zero" cells, one of them contributing to $2v$

$$CN = \frac{N_{\mathrm{ROI}}}{8v}\frac{5v}{R}\frac{R}{6} = \frac{5N_{\mathrm{ROI}}}{48}. \tag{D.8}$$

Interestingly, anyway, in this situation it is possible to include all non-zero cells in a $L = 2R$ radius ball, which would have $N_{\mathrm{ROI}} = 13$ (Fig. 25 (B)) and thus CN close to 1 (65/48).

D.2. Continuous approach

Models using a velocity field defined on a continuous scale smaller than R have little physical or computational value, but allowing for analytical computations, they are helpful in better clarifying basic concepts. Let us generalise Eq. (8) to

$$\mathbf{v}(r, \varphi) = \frac{v_R}{R} f(r) \mathbf{e}_\varphi. \tag{D.9}$$

so that

$$(\nabla \times \mathbf{v})_z = \frac{v_R}{rR}\partial_r\left(rf(r)\right) \equiv \frac{v_R}{rR}\partial_r\left(g(r)\right), \tag{D.10}$$

where we defined

$$g(r) \equiv rf(r). \tag{D.11}$$

Now, if $f(r) = r$, we have (Eq. (9)) $(\nabla \times \mathbf{v})_z = 2v_R/R$, so we may define

$$\mathrm{Rot}^{\mathrm{Max}} = \frac{2v_R}{R}. \tag{D.12}$$

Furthermore, we define $l(r)$ such that

$$(\nabla \times \mathbf{v})_z \equiv \mathrm{Rot}^{\mathrm{Max}} l(r), \tag{D.13}$$

and as a consequence

$$h(r) \equiv 2rl(r) = \partial_r\left(g(r)\right), \tag{D.14}$$

which gives us a differential equation for the value of the velocity field given the value of the rotor one. Furthermore, we have, on a disc D_r,

$$\langle v\rangle_{D_r} = \frac{(v_R/R)\int_0^{2\pi}\mathrm{d}\varphi\int_0^r f(\rho)\rho\,\mathrm{d}\rho}{\pi r^2} = \frac{(v_R/R)2\pi\int_0^r f(\rho)\rho\,\mathrm{d}\rho}{\pi r^2} = \frac{\mathrm{Rot}^{\mathrm{Max}}}{r^2}\int_0^r f(\rho)\rho\,\mathrm{d}\rho. \tag{D.15}$$

D.2.1. Continuous rotor field

Let us assume now that between two maximally rotating fields the value of the rotor passes gradually from $2v_R/R$ to $-2v_R/R$ in a $2R$ distance. This may be attained by using the following function for $l(r)$

$$l(r) = \begin{cases} 1, & \text{if } 0 \le r < R \\ 2 - \frac{r}{R}, & \text{if } R \le r < 2R \\ 0, & \text{if } r \ge 2R \end{cases} \tag{D.16}$$

or

$$h(r) = \begin{cases} 2r, & \text{if } 0 \le r < R \\ 4r - \frac{2r^2}{R}, & \text{if } R \le r < 2R \\ 0, & \text{if } r \ge 2R \end{cases} \tag{D.17}$$

The function is clearly not differentiable in R and $2R$, but a differentiable version in which the radial derivative of h transits from 0 to $-1/R$ (and vice versa in $2R$) in a $\lambda \ll R$ scale can be obtained using a "smoothed step function", adapting the detailed description on bump functions found in W. Tu (2011).

Using

$$g(r) = \int_0^r h(\rho)\,\mathrm{d}\rho \tag{D.18}$$

we obtain

$$g(r) = \begin{cases} r^2, & \text{if } 0 \le r < R \\ 2r^2 - \frac{2r^3}{3R} - \frac{R^2}{3}, & \text{if } R \le r < 2R \\ \frac{7R^2}{3}, & \text{if } r \ge 2R \end{cases} \tag{D.19}$$

or

$$f(r) = \begin{cases} r, & \text{if } 0 \le r < R \\ 2r - \frac{2r^2}{3R} - \frac{R^2}{3r}, & \text{if } R \le r < 2R \\ \frac{7R^2}{3r}, & \text{if } r \ge 2R \end{cases} \tag{D.20}$$

and

$$\langle v\rangle_{D_r} = \begin{cases} \mathrm{Rot}^{\mathrm{Max}}\frac{r}{3}, & \text{if } 0 \le r < R \\ \mathrm{Rot}^{\mathrm{Max}}(\frac{2r}{3} - \frac{r^2}{6R} - \frac{R^2}{3r} + \frac{R^3}{6r^2}), & \text{if } R \le r < 2R \\ \mathrm{Rot}^{\mathrm{Max}}\frac{R^2(14r-15R)}{6r^2}, & \text{if } r \ge 2R. \end{cases} \tag{D.21}$$

We introduced this model because it reproduces our "linear approximation" for the gradient, so we may use it to check the validity of the approximation according to which $\langle v\rangle_{\mathrm{ROI}} = 2/3 v_R$. Using the above results, for $2R$ we obtain $\langle v\rangle_{D_{2R}} = 13/12 v_R$. In the case of two different opposing rotating fields, we may use as ROI a disc of radius $4R$ located in the middle point. A numerical integration gives for this case $\langle v\rangle_{D_{4R}} \approx 1.0095 v_R$. These values suggest again that the maximal possible CN value should not depart strongly from 1.

D.2.2. Discontinuous rotor field

Defining the velocity field starting from the rotor may seem counter-intuitive. We could have started from the velocity field, e.g., asking the velocity to be zero outside a disc of radius $2R$

$$f(r) = \begin{cases} r, & \text{if } 0 \le r < R \\ 2R - r, & \text{if } R \le r < 2R \\ 0, & \text{if } r \ge 2R \end{cases} \tag{D.22}$$

By straightforward differentiation we have now

$$l(r) = \begin{cases} 1, & \text{if } 0 \le r < R \\ \frac{R}{r} - 1, & \text{if } R \le r < 2R \\ 0, & \text{if } r \ge 2R \end{cases} \tag{D.23}$$

The rotor field is now discontinuous. The continuity can be regained by using bump functions (W. Tu, 2011) in such a way that $f(r)$ is re-defined as a differentiable function in R, i.e. by having $l(r)$ to make a continuous transition from 1 to 0 over a scale $\lambda \ll R$. Anyway, in this way the gradient of the rotor would be increased by a scale R/λ with respect to the "macroscopic variation" scale v_R/R^2. This toy model serves thus to remind us that trying to define the differential congestion (DC and EDC) on a scale smaller than R is meaningless, and justifies our use of a linear approximation, i.e. of the comparison between the maximum and minimum values on the ROI.

By integrating $f(r)$ we obtain for this model

$$\langle v\rangle_{D_r} = \begin{cases} \mathrm{Rot}^{\mathrm{Max}} \frac{r}{3}, & \text{if } 0 \le r < R \\ \mathrm{Rot}^{\mathrm{Max}} (R - \frac{r}{3} - \frac{R^3}{3r^2}), & \text{if } R \le r < 2R \\ \mathrm{Rot}^{\mathrm{Max}} \frac{R^3}{r^2}, & \text{if } r \ge 2R \end{cases} \tag{D.24}$$

The result for $r > 2R$ is the mathematical average, but since the velocity for $r > 2R$ is zero, the average according to the CL definition is the $2R$ value, or $\langle v\rangle = v_R/2$. If the velocity for $r > 2R$ is negligible but non-zero, for two opposite flows included in a D_{4R} ROI, we have $\langle v\rangle = v_R/4$ and $CN = 8/3$, showing that also for continuous models we may have CN quite large in these seemingly artificial settings.

References

Atienza-Vanacloig, V., Rosell-Ortega, J., Andreu-Garcia, G., Valiente-González, J., 2008. People and luggage recognition in airport surveillance under real-time constraints. In: International Conference on Pattern Recognition. IEEE, pp. 1–4. http://dx.doi.org/10.1109/ICPR.2008.4761004.

Boltes, M., 2015. Automatische Erfassung präziser Trajektorien in Personenströmen hoher Dichte (Ph.D. thesis). (FZJ-2015-01334), Jülich Supercomputing Center.

Brščić, D., Kanda, T., Ikeda, T., Miyashita, T., 2013. Person tracking in large public spaces using 3-D range sensors. IEEE Trans. Hum.-Mach. Syst. 43 (6), 522–534.

Brščić, D., Zanlungo, F., Kanda, T., 2014. Density and velocity patterns during one year of pedestrian tracking. Transp. Res. Procedia 2, 77–86.

Cai, L., Zhu, J., Zeng, H., Chen, J., Cai, C., Ma, K.-K., 2018. HOG-assisted deep feature learning for pedestrian gender recognition. J. Franklin Inst. B 355 (4), 1991–2008. http://dx.doi.org/10.1016/j.jfranklin.2017.09.003.

Cheung, C., Lam, W.H., 1998. Pedestrian route choices between escalator and stairway in MTR stations. J. Transp. Eng. 124 (3), 277–285. http://dx.doi.org/10.1061/(ASCE)0733-947X(1998)124:3(277).

Corbetta, A., Meeusen, J.A., Lee, C.-M., Benzi, R., Toschi, F., 2018. Physics-based modeling and data representation of pairwise interactions among pedestrians. Phys. Rev. E 98 (6), 062310.

Elliott, D., Smith, D., 1993. Football stadia disasters in the United Kingdom: learning from tragedy? Ind. Environ. Crisis Q. 7 (3), 205–229. http://dx.doi.org/10.1177/108602669300700304.

Feliciani, C., Hisashi, M., Katsuhiro, N., 2022. Perpendicular crossflow experiment with partial information on body orientation. http://dx.doi.org/10.34735/ped.2019.2.

Feliciani, C., Murakami, H., Nishinari, K., 2018. A universal function for capacity of bidirectional pedestrian streams: Filling the gaps in the literature. PLoS One 13 (12), e0208496. http://dx.doi.org/10.1371/journal.pone.0208496.

Feliciani, C., Nishinari, K., 2018a. Estimation of pedestrian crowds' properties using commercial tablets and smartphones. Transp. B Transp. Dyn. http://dx.doi.org/10.1080/21680566.2018.1517061.

Feliciani, C., Nishinari, K., 2018b. Measurement of congestion and intrinsic risk in pedestrian crowds. Transp. Res. C 91, 124–155. http://dx.doi.org/10.1016/j.trc.2018.03.027.

Feliciani, C., Nishinari, K., 2020. Investigation of pedestrian evacuation scenarios through congestion level and crowd danger. Collect. Dyn. 5, 150–157. http://dx.doi.org/10.17815/CD.2020.45.

Feliciani, C., Zuriguel, I., Garcimartín, A., Maza, D., Nishinari, K., 2020a. Systematic experimental investigation of the obstacle effect during non-competitive and extremely competitive evacuations. Sci. Rep. 10 (1), 1–20. http://dx.doi.org/10.1038/s41598-020-72733-w.

Feliciani, C., Zuriguel, I., Garcimartin, A., Maza, D., Nishinari, K., 2020b. Systematic experimental investigation of the obstacle effect during non-competitive and extremely competitive evacuations. Sci. Rep. 10, 15947. http://dx.doi.org/10.1038/s41598-020-72733-w.

Frankel, T., 2011. The Geometry of Physics: An Introduction. Cambridge University Press.
Fruin, J.J., 1971. Pedestrian Planning and Design. Elevator Books.
Fujita, A., Feliciani, C., Yanagisawa, D., Nishinari, K., 2019. Traffic flow in a crowd of pedestrians walking at different speeds. Phys. Rev. E 99 (6), 062307. http://dx.doi.org/10.1103/PhysRevE.99.062307.
Haghani, M., 2020a. Empirical methods in pedestrian, crowd and evacuation dynamics: Part I. Experimental methods and emerging topics. Saf. Sci. 129, 104743. http://dx.doi.org/10.1016/j.ssci.2020.104743.
Haghani, M., 2020b. Empirical methods in pedestrian, crowd and evacuation dynamics: Part II. Field methods and controversial topics. Saf. Sci. 129, 104760. http://dx.doi.org/10.1016/j.ssci.2020.104760.
Hassner, T., Itcher, Y., Kliper-Gross, O., 2012. Violent flows: Real-time detection of violent crowd behavior. In: IEEE Computer Society Conference on Computer Vision and Pattern Recognition Workshops. IEEE, pp. 1–6. http://dx.doi.org/10.1109/CVPRW.2012.6239348.
Helbing, D., Johansson, A., Al-Abideen, H.Z., 2007. Dynamics of crowd disasters: An empirical study. Phys. Rev. E 75 (4), 046109. http://dx.doi.org/10.1103/PhysRevE.75.046109.
Hosseini, O., Maghrebi, M., Maghrebi, M.F., 2021. Determining optimum staged-evacuation schedule considering total evacuation time, congestion severity and fire threats. Saf. Sci. 139, 105211. http://dx.doi.org/10.1016/j.ssci.2021.105211.
Huang, L., Chen, T., Wang, Y., Yuan, H., 2015. Congestion detection of pedestrians using the velocity entropy: A case study of Love Parade 2010 disaster. Physica A 440, 200–209. http://dx.doi.org/10.1016/j.physa.2015.08.013.
Illiyas, F.T., Mani, S.K., Pradeepkumar, A., Mohan, K., 2013. Human stampedes during religious festivals: A comparative review of mass gathering emergencies in India. Int. J. Disaster Risk Reduct. 5, 10–18. http://dx.doi.org/10.1016/j.ijdrr.2013.09.003.
Kok, V.J., Lim, M.K., Chan, C.S., 2016. Crowd behavior analysis: A review where physics meets biology. Neurocomputing 177, 342–362. http://dx.doi.org/10.1016/j.neucom.2015.11.021.
Kratz, L., Nishino, K., 2009. Anomaly detection in extremely crowded scenes using spatio-temporal motion pattern models. In: IEEE Conference on Computer Vision and Pattern Recognition. IEEE, pp. 1446–1453. http://dx.doi.org/10.1109/CVPR.2009.5206771.
Lam, W.H., Cheung, C.-Y., 2000. Pedestrian speed/flow relationships for walking facilities in hong kong. J. Transp. Eng. 126 (4), 343–349. http://dx.doi.org/10.1061/(ASCE)0733-947X(2000)126:4(343).
Lautrup, B., 2011. Physics of Continuous Matter: Exotic and Everyday Phenomena in the Macroscopic World. CRC Press.
Lin, J.-W., Lu, M.-H., Lin, Y.-H., 2019. A thermal camera based continuous body temperature measurement system. In: IEEE International Conference on Computer Vision Workshops. pp. 1–7.
Lovreglio, R., Ronchi, E., Kinsey, M.J., 2019. An online survey of pedestrian evacuation model usage and users. Fire Technol. 1–21. http://dx.doi.org/10.1007/s10694-019-00923-8.
Masoud, O., Papanikolopoulos, N.P., 2001. A novel method for tracking and counting pedestrians in real-time using a single camera. IEEE Trans. Veh. Technol. 50 (5), 1267–1278. http://dx.doi.org/10.1109/25.950328.
Mathworks, 2022. Lowess smoothing. URL https://mathworks.com/help/curvefit/lowess-smoothing.html.
Munirajulu, M., 2018. Autodesk CFD for Fire and Smoke Simulation in Buildings. Autodesk, URL https://www.autodesk.com/autodesk-university/class/Autodesk-CFD-Fire-and-Smoke-Simulation-Buildings-2018.
Nievas, E.B., Suarez, O.D., García, G.B., Sukthankar, R., 2011. Violence detection in video using computer vision techniques. In: International Conference on Computer Analysis of Images and Patterns. Springer, pp. 332–339. http://dx.doi.org/10.1007/978-3-642-23678-5_39.
Nowak, S., Schadschneider, A., 2012. Quantitative analysis of pedestrian counterflow in a cellular automaton model. Phys. Rev. E 85 (6), 066128. http://dx.doi.org/10.1103/PhysRevE.85.066128.
Ravishankar, S., Mahr, K., Birsel, R., 2015. Stampede at religious festival in Andhra kills 27 pilgrims. Reuters, https://www.reuters.com/article/stampede-rajahmundry-mahapushkaralu/stampede-at-religious-festival-in-andhra-kills-27-pilgrims-idUKKCN0PO0O520150714.
Rogsch, C., Schreckenberg, M., Tribble, E., Klingsch, W., Kretz, T., 2010. Was it panic? An overview about mass-emergencies and their origins all over the world for recent years. In: Pedestrian and Evacuation Dynamics 2008. Springer, pp. 743–755. http://dx.doi.org/10.1007/978-3-642-04504-2_72.
Rokko High School, 2017. Rokko High School Sport Festival 2017: marching parade. Youtube, https://youtu.be/Sd5xV5RtF1A?t=610. 2020-11-16.
Schauer, L., Werner, M., Marcus, P., 2014. Estimating crowd densities and pedestrian flows using wi-fi and bluetooth. In: International Conference on Mobile and Ubiquitous Systems: Computing, Networking and Services. pp. 171–177. http://dx.doi.org/10.4108/icst.mobiquitous.2014.257870.
Shiwakoti, N., Shi, X., Ye, Z., 2019. A review on the performance of an obstacle near an exit on pedestrian crowd evacuation. Saf. Sci. 113, 54–67.
Szarvas, M., Sakai, U., Ogata, J., 2006. Real-time pedestrian detection using LIDAR and convolutional neural networks. In: IEEE Intelligent Vehicles Symposium. IEEE, pp. 213–218.
Van der Spek, S., Van Schaick, J., De Bois, P., De Haan, R., 2009. Sensing human activity: GPS tracking. Sensors 9 (4), 3033–3055. http://dx.doi.org/10.3390/s90403033.
Vendelø, M.T., 2019. The past, present and future of event safety research. In: A Research Agenda for Event Management. Edward Elgar Publishing, http://dx.doi.org/10.4337/9781788114363.00010.
W. Tu, L., 2011. An Introduction to Manifolds. Springer.
Weidmann, U., 1993. Transporttechnik der Fussgänger: Transporttechnische Eigenschaften des Fussgängerverkehrs (Literaturauswertung). ETH, IVT, http://dx.doi.org/10.3929/ethz-a-000687810.
Wikipedia, 2020. List of human stampedes and crushes. https://en.wikipedia.org/wiki/List_of_human_stampedes_and_crushes.
Yamori, K., 1998. Going with the flow: Micro–macro dynamics in the macrobehavioral patterns of pedestrian crowds. Psychol. Rev. 105 (3), 530. http://dx.doi.org/10.1037/0033-295X.105.3.530.
Ye, R., Fang, Z., Lian, L., Wang, Q., Zeng, G., Cao, S., Zhang, J., Song, W., 2021. Traffic dynamics of uni-and bidirectional pedestrian flows including dyad social groups in a ring-shaped corridor. J. Stat. Mech. Theory Exp. 2021 (2), 023406. http://dx.doi.org/10.1088/1742-5468/abdc1a.
Ye, R., Zhan, Z., Chraibi, M., Lian, L., Zhang, J., Song, W., 2020. Investigating the effect of stairs on the bidirectional movement of pedestrians. J. Stat. Mech. Theory Exp. 2020 (2), 023405. http://dx.doi.org/10.1088/1742-5468/ab6b1a.
Yücel, Z., Zanlungo, F., Feliciani, C., Gregorj, A., Kanda, T., 2019. Identification of social relation within pedestrian dyads. PLoS One 14 (10), e0223656.
Yücel, Z., Zanlungo, F., Ikeda, T., Miyashita, T., Hagita, N., 2013. Deciphering the crowd: Modeling and identification of pedestrian group motion. Sensors 13 (1), 875–897.
Zanlungo, F., 2007. A collision-avoiding mechanism based on a theory of mind. Adv. Complex Syst. 10 (supp02), 363–371.
Zanlungo, F., 2020. CN computation. https://github.com/yucelzeynep/A-pure-number-to-assess-congestion-in-pedestrian-crowds, 2020-10-27.
Zanlungo, F., Brščić, D., Kanda, T., 2015. Spatial-size scaling of pedestrian groups under growing density conditions. Phys. Rev. E 91 (6), 062810.
Zanlungo, F., Crociani, L., Yücel, Z., Kanda, T., 2019a. The effect of social groups on the dynamics of bi-directional pedestrian flow: A numerical study. arXiv preprint arXiv:1910.04337.
Zanlungo, F., Feliciani, C., Yücel, Z., Nishinari, K., Kanda, T., 2023a. Macroscopic and microscopic dynamics of a pedestrian cross-flow: Part I, experimental analysis. Saf. Sci. 158, 105953.
Zanlungo, F., Feliciani, C., Yücel, Z., Nishinari, K., Kanda, T., 2023b. Macroscopic and microscopic dynamics of a pedestrian cross-flow: Part II, modelling. Saf. Sci. 158, 105969.

Zanlungo, F., Ikeda, T., Kanda, T., 2012. A microscopic "social norm" model to obtain realistic macroscopic velocity and density pedestrian distributions. PLoS One 7 (12), e50720.

Zanlungo, F., Yücel, Z., Brščić, D., Kanda, T., Hagita, N., 2017. Intrinsic group behaviour: Dependence of pedestrian dyad dynamics on principal social and personal features. PLoS One 12 (11), e0187253.

Zanlungo, F., Yücel, Z., Kanda, T., 2019b. Intrinsic group behaviour II: On the dependence of triad spatial dynamics on social and personal features; and on the effect of social interaction on small group dynamics. PLoS One 14 (12), e0225704.

Zhang, J., Klingsch, W., Schadschneider, A., Seyfried, A., 2012. Ordering in bidirectional pedestrian flows and its influence on the fundamental diagram. J. Stat. Mech. Theory Exp. 2012 (02), P02002. http://dx.doi.org/10.1088/1742-5468/2012/02/P02002.